Electrochimica Acta 391 (2021) 138975

Contents lists available at ScienceDirect

Electrochimica Acta

journal homepage: www.elsevier.com/locate/electacta

Voltammetric and electrochemical impedance analysis of poly(bisphenol A) supported poly(3,4-ethylenedioxythiophene) layers deposited on gold – the effects of thickness distribution, overoxidation and non-stationarity

Krisztina J. Szekeres, Mária Ujvári, Soma Vesztergom, Győző G. Láng*

Institute of Chemistry, Laboratory of Electrochemistry and Electroanalytical Chemistry, Eötvös Loránd University, Pázmány Péter sétány 1/A, Budapest H-1117, Hungary

ARTICLE INFO

Article history:
Received 10 May 2021
Revised 15 July 2021
Accepted 18 July 2021
Available online 28 July 2021

Keywords:
Polymer modified electrodes
Poly(3,4-ethylenedioxythiophene) (PEDOT) and poly(bisphenol A) (PBA)
Overoxidation
Non-stationarity
Electrochemical impedance spectroscopy (EIS)

ABSTRACT

The present study describes the preparation and electrochemical characterization of poly(bisphenol A) (poly(BPA)) supported poly(3,4-ethylenedioxythiophene) (PEDOT) modified gold electrodes.

Cyclic voltammetry (CV) and electrochemical impedance spectroscopy (EIS) were used to characterize the electrochemistry of the Au | PEDOT | 0.1 mol/dm^3 H_2SO_4(aq.) and Au | [poly(BPA)/PEDOT] | 0.1 mol/dm^3 H_2SO_4(aq.) electrodes before and after overoxidation. Scanning electron microscopy (SEM) was used for the study of the structure/morphology of the polymer coatings.

Similarly to overoxidized PEDOT modified electrodes, time evolution of the electrochemical properties of the poly(BPA)/PEDOT films could be observed after overoxidation. The four-dimensional (4D) analysis method (i.e., a post-experimental mathematical/analytical procedure to overcome the problems caused by non-stationarity) and complex nonlinear least-squares (CNLS) fitting has been used for the estimation of the impedance parameters corresponding to different time instants after overoxidation of the [poly(BPA)/PEDOT] film.

The deviations of the impedance responses from the purely capacitive behavior predicted at low frequencies by the theoretical models could be well explained solely by the assumption of uneven film thickness. It has been found that the impedance model, which takes into account the film thickness distribution gives a good description of the impedance data, both before and after overoxidation.

According to the results, after the electrochemical deposition of poly(BPA) on the PEDOT layer the resulting [poly(BPA)/PEDOT] modified electrode becomes more resistant against the negative effects of overoxidation.

1. Introduction

Organic conductors are often used in different kind of practical applications such as electronic, electrochromic, optical sensors and devices [1,2]. Compared to other conductors, there are some advantages by using conducting polymers and its composites: this type of polymeric materials exhibits superior flexibility, they can be easily modified and combined. Conducting polymer films can be deposited directly onto the surface of a conductive substrate by electrochemical methods while the substrate is immersed in an electrolyte solution containing monomer molecules. Nevertheless, after almost half a century of intensive research in the field of electrochemically active, electronically conducting polymeric systems, some aspects of their electrochemical behavior are still not fully understood [3–5].

Poly(3,4-ethylenedioxythiophene) (PEDOT) belongs to the family of conducting polymers with high electronic conductivity, good chemical stability, controllable optoelectronic and redox properties. The alkylenedioxy substitution pattern serves to enhance the electrochemical, optical, and electrochromic properties of the polythiophene backbone. PEDOT is therefore an often-used conductive polymer in sensors. It can be found in TNT sensors [6], hydrogen chloride and ammonia vapor detectors [7], NO_2 sensors [8], neural probes [9], uric acid and dopamine sensors [10,11], and a

* Corresponding author.
E-mail address: langgyg@chem.elte.hu (G.G. Láng).

https://doi.org/10.1016/j.electacta.2021.138975

bunch of other medical biosensors [12]. Connecting electronics directly to human tissues in the body ("cyborg technology") is a huge challenge. Traditional optoelectronic and microelectronic materials, such as semiconductors, gold, iridium, or stainless steel may cause scarring when implanted. For applications in living tissue, electrical signals need to be transmitted between the implant and the tissue to operate properly, but scars interrupt this activity. According to recent results PEDOT dramatically improved the performance of medical implants by lowering their impedance two to three orders of magnitude [13,14].

It should be noted, however, that in these devices PEDOT is often in the so called "overoxidized" state (or turns to this state during operation). In studies performed to investigate the electrochemistry of PEDOT in more detail by using cyclic voltammetry (CV) it has been found that when the positive potential limit of the CV is extended into the region in which the "overoxidation" of the polymer film takes place, an oxidation peak (without a corresponding reduction peak) appears [15–22]. According to experimental results, the mechano-electrochemical properties of conductive polymers may change significantly during oxidation or reduction processes [23–25]. The same is true for PEDOT layers in polymer modified electrodes. Note that a polymer in different overoxidation states may have beneficial properties as well, for example, increased porosity and higher affinity for adsorption of different substances [18,26]. Unfortunately, overoxidation is very often accompanied by delamination at the film/substrate interface making the unit unusable. The fracture generally starts with growth of a flaw on the film surface and continues with channel cracking in the film [17,19].

To solve this problem, we need to find a solution that could keep the electrochemical properties, especially conductivity, of the PEDOT polymer practically intact while changing the mechanical properties of the layer in order to make it more resistant against the effects of overoxidation. In a recent study on the electrochemical behavior of bisphenol A (BPA) at a gold | 0.1 M sodium perchlorate electrode it was found that during the cycling of the electrode potential an adherent, flexible and poorly conducting poly(bisphenol A) (pBPA) film was formed on the gold surface [27]. This result is in line with previous studies which showed that the electrochemical oxidation of phenolic compounds causes the inactivation of graphite, glassy carbon (GC) or noble metal electrodes [28–31]. On the other hand, the redox activity exhibited by a poly(BPA) film coated on a PEDOT-modified glassy carbon electrode has been proposed to determine the concentration of BPA in aqueous solutions, however, the removal of the poly(BPA) film from electrode substrates presented difficulty for subsequent measurements [32,33].

Based on the above findings, the idea arose that the mechanical properties of a PEDOT layer and its resistance against the consequences of overoxidation could be improved by the electrochemical deposition of poly(BPA) on its surface and in its pores, i.e. by the combination of the two polymers. This procedure looks promising in terms of mechanical properties, however, to date, no results have been reported on the electrochemical performance of the "combined" film. It is known that pure poly(BPA) has low electrochemical conductivity and poor electrochemical activity [27], therefore, it was expected that its presence would not affect considerably the electrochemical properties of the PEDOT layer, even after its overoxidation.

The most commonly used methods for the electrochemical characterization of polymer modified electrodes are cyclic voltammetry (CV) and electrochemical impedance spectroscopy (EIS). For instance, comparison of the charge transfer resistances and other characteristic EIS parameters of PEDOT and poly(BPA)/PEDOT modified electrodes can reveal the difference between the electrochemical properties of the two systems. In principle, the same methods can also be used for the investigation of the electrochemical properties of electrodes modified with overoxidized poly(BPA)/PEDOT layers. Unfortunately, time evolution of the impedance response is a common feature of electrodes containing overoxidized PEDOT [19–22,34]. According to this observation, the sequentially recorded sets of experimental data (i.e. the impedances measured in the frequency range of 10 kHz–0.01 Hz using the consecutive frequency sweep mode) change slowly, but continuously over several hours when the electrode potential is held in the "stability region" after overoxidation of the film. By comparing the properties of the GC|PEDOT|0.1 M H_2SO_4 and the Au|PEDOT|0.1 M H_2SO_4 electrodes a mechanistic explanation for the observed behavior has been proposed in [22]. However, according to the usual interpretation of the concept of impedance, impedance is not defined as time-dependent and, therefore, there should not exist an impedance out of stationary conditions. This means that if the requirement of stationarity in impedance spectroscopy is in conflict with the essential properties of the object, the measured data points are not "impedances", the obtained sets of experimental data are not "impedance spectra" and they can hardly be used in any analysis based on traditional impedance models. On the other hand, under some suitable conditions time dependence can be conciliated into the concept of impedance [20,21,35–39]. The so-called "four-dimensional analysis" is one of the methods proposed for correction of the systematic errors, arising during the measurements of time-evolving impedance [40–42], i.e. when the consecutive impedance measurements are performed at different system states, but each of the measured impedance values can be accepted as "valid", at least approximately, in the classical sense. This is equivalent to the assumption that only insignificant changes in the system occur during the time required for measurement of a single impedance data point. The four-dimensional analysis (FDA) method assumes the continuity of parameters in the space spanned by the variables f (or ω), Re(Z), Im(Z) and t (i.e. frequency or angular frequency, real and imaginary parts of the impedance, and time). This means that every measured data should additionally contain the time of the measurement. By taking advantage of the continuity of the evolution, interpolation is performed resulting in instantaneous projections of the full impedance-time space and "reconstructed" impedances related to a selected instant of the time. Each of these diagrams can be regarded as a stationary one, free of non-steady-state errors (at least approximately). If the problem is related to the mathematical basis of the transfer function analysis, other methods, such as windowing techniques should be used [39].

Unfortunately, non-stationary behavior of the system is not the only issue one faces when attempting to evaluate impedance data obtained for PEDOT or poly(BPA)/PEDOT modified electrodes, the nonuniform film thickness causes further complications. The problem of thickness distribution of polymer films in modified electrodes has been addressed in several papers [43–47], only few studies have focused on the development of "complete" impedance models which allow the simultaneous estimation of impedance parameters by fitting experimental data in wide frequency ranges.

The aim of the present study was the preparation and electrochemical characterization of Au | [poly(BPA)/PEDOT] | 0.1 mol/dm^3 H_2SO_4(aq.) electrodes. Scanning electron microscopy (SEM) has been used for the study of the structure/morphology of the polymer coatings. The electrochemistry of the polymer modified electrodes before and after overoxidation has been investigated by cyclic voltammetry and electrochemical impedance spectroscopy (EIS). The four-dimensional analysis method and complex nonlinear least-squares (CNLS) fitting has been used for the estimation of the impedance parameters corresponding to time instants after overoxidation of the polymer film. The effects of thickness distribution have been taken into account in the impedance expression used in CNLS fitting of the experimental EIS data.

2. Experimental

2.1. Reagents

3,4-Ethylenedioxythiophene (EDOT) and Bisphenol A (BPA) were purchased from Aldrich and Aldrich-Chemie, respectively. All chemical reagents were used as received without further purification. All solutions were prepared with ultrapure water (Milli-Q®, specific resistance: 18.2 $M\Omega \cdot cm^{-1}$). Reagent grade sulfuric acid (Merck) and sodium sulfate decahydrate (VWR) were used for the preparation of 0.01 $mol \cdot dm^{-3}$ EDOT/0.1 $mol \cdot dm^{-3}$ Na_2SO_4 (aq.) and 100 ppm BPA/0.5 $mol \cdot dm^{-3}$ H_2SO_4 (aq.) solutions. The polymer films were formed on gold discs (Metal-Art 0.9999, projected area, $A = 0.196$ cm^2). Before electrodeposition, the gold surface was polished by 1 μm diamond suspension (Struers DP). The roughness factor of the gold electrodes (calculated from the charge associated with the oxide formation on the gold surface) was $f_r \approx 2$. All electrochemical measurements were carried out at room temperature (22.0 ± 0.5) °C. The solutions were purged with oxygen-free argon (Linde 5.0) before use, and an inert gas blanket was maintained throughout the experiments.

2.2. Apparatus

A Zahner IM6 electrochemical workstation (controlled by the Thales software package) was used in all electrochemical measurements. The impedance measurements were performed using single sine excitation at 57 discrete frequencies ('frequency by frequency' mode) in the frequency range of 96.1 mHz–50 kHz by applying an AC amplitude of 5 mV rms.

A Quanta™ 3D FEG high-resolution dual beam scanning electron microscopy (SEM/FIB) with silicon drift X-ray detector (EDX) instrument was used for SEM and elemental analysis. Both secondary and backscattered electrons were used to obtain the respective images. The characterization included focused ion beam (FIB) cross section imaging, as well. A gallium liquid metal ion source (LMIS) was used to create a cross-section cut on the sample surface. Unlike the electron microscope, the FIB is inherently destructive for the specimen. A layer of ion beam deposited one-micrometer thick platinum was applied to the surface of each sample prior to milling with the intention to protect and preserve the polymer layer and to avoid Ga contamination. The Ga ion cutting (incision) was performed perpendicular to the sample surface. The properties of the ion beam used for this process was 30 kV high voltage and 3 nA beam current.

2.3. Preparation and electrochemical characterization of PEDOT- and poly(BPA)/PEDOT-modified gold electrodes

The preparation and electrochemical characterization of PEDOT- and poly(BPA)/PEDOT-modified gold electrodes have been carried out according to the following steps:

- Step 1–deposition of the PEDOT layers

Electrodeposition of PEDOT layers was carried out in a common three electrode cell in which the working electrode was a gold disc ($A = 0.196$ cm^2, see above) in contact with freshly prepared 0.01 mol•$\cdot dm^{-3}$ EDOT / 0.1 $mol \cdot dm^{-3}$ Na_2SO_4 solution, the counter electrode was a ring-shaped Pt wire immersed into the same solution, and a KCl-saturated calomel electrode (SCE) was used as reference electrode. During the galvanostatic deposition $j = 0.2$ mA/cm^2 current density was used. The deposition time was $t = 1800$ s or $t = 3600$ s (3-3 PEDOT modified gold electrodes have been prepared under identical conditions, except for the deposition time, called samples E1-E3 (deposition time: $t = 1800$ s) and F1–F3, respectively (deposition time: $t = 3600$ s)).

After the deposition, the polymer layer was left for one-day relaxation in ultrapure ("Milli-Q®") water.

- Step 2–investigation of the PEDOT-modified electrodes

Investigation of PEDOT layers was carried out in common three electrode cell in which the working electrode was a gold plate ($A = 0.196$ cm^2) with the deposited PEDOT layer in contact with 0.5 mol/dm^3 H_2SO_4 solution, the counter electrode was a ring-shaped Pt plate immersed into the same solution. A NaCl-saturated calomel electrode (SSCE) was used as reference electrode.

The potential range during the cyclic voltammetric measurements was $E = (-0.1–0.8)$ V *vs.* SSCE (samples E1–E3) or $E = (-0.4–1.0)$ V *vs.* SSCE (samples F1–F3), the scan rate was $v = 50$ mV/s or $v = 100$ mV/s.

Impedance measurements were performed on sample E1 in 0.1 mol/dm^3 H_2SO_4 solution in the frequency range of 50 kHz–96.1 mHz (amplitude of the perturbing signal: 5 mV rms, electrode potential $E = 0.4$ V *vs.* SSCE). A high surface area gold-foil (immersed in the 0.1 mol/dm^3 H_2SO_4 solution) was arranged cylindrically around the working electrode to maintain a uniform electric field (counter electrode). The reference electrode was a saturated sodium calomel electrode (SSCE). The linearity of the system has been checked by comparing the impedance spectra obtained with different amplitudes (ranging from 1 to 5 mV rms)

- Step 3–deposition of poly(BPA)

Electrodeposition of poly(BPA) was carried out in common three electrode cell in which the working electrode was a gold plate ($A = 0.196$ cm^2) with deposited PEDOT layer in contact with a 100 ppm BPA / 0.5 $mol \cdot dm^{-3}$ H_2SO_4 solution, the counter electrode was a Pt wire immersed into the same solution, and SSCE was used as reference electrode. The potentiodynamic electrodeposition was performed in the potential window of $E = (-0.1$ V–1.0) V *vs.* SSCE (samples E1and E2) or $E = (-0.4$ V–1.0) V *vs.* SSCE (samples F1 and F2), the scan rate was $v = 100$ mV/s, the number of cycles was 10.

After the deposition, the poly(BPA) supported PEDOT layer was left for one-day relaxation in ultrapure water.

- Step 4 – investigation of the poly(BPA)/PEDOT-modified electrodes

Investigation of poly(BPA)/PEDOT layer was carried out in common three electrode cell in which the working electrode was a gold plate (samples E1 and F1, $A = 0.196$ cm^2) with the deposited poly(BPA)/PEDOT layer in contact with 0.1 mol/dm^3 H_2SO_4 solution, the counter electrode was a ring-shaped Pt plate immersed in the same solution, and the reference electrode was SSCE.

The potential range during the cyclic voltammetric measurements was $E = (-0.1–0.8)$ V vs. SSCE (sample E1) or $E = (-0.4–1.0)$ V *vs.* SSCE (sample F1), the scan rate was $v = 50$ mV/s or $v = 100$ mV/s.

Electrochemical impedance measurements were performed on sample E1 in 0.1 mol/dm^3 H_2SO_4 solution in the frequency range of 50 kHz–96.1 mHz (amplitude of the perturbing signal: 5 mV rms, electrode potential $E = 0.4$or 0.2 V *vs.* SSCE). The cell geometry was the same as that described in Step 2. Linearity of the impedance response was analyzed as previously described (Step 2) using different AC perturbation amplitudes.

- Step 5–overoxidation of the PEDOT and poly(BPA)/PEDOT layers

The overoxidation of the poly(BPA)/PEDOT layers was carried out in a common three electrode cell in which the working electrode was the PEDOT+poly(BPA) modified gold electrode (sample E1 and F1) or the PEDOT modified gold electrode (samples E3

and F3), the reference electrode was SSCE, and the counter electrode was a ring-shaped Pt plate. Electrolyte solution: 0.1 mol/dm^3 H_2SO_4(aq.).

The potential range of the potentiodynamic/cyclic voltammetric (over)oxidation was E = (0.4–1.5) V *vs.* SSCE (sample E1 and E3) or E = (–0.4–1.5) V *vs.* SSCE (sample F1 and F3) the scan rate was v = 50 mV/s, number of cycles: 3.

- Step 6–Electrochemical impedance study of the poly(BPA)/PEDOT layer after overoxidation

Investigation of the overoxidized poly(BPA)/PEDOT layer was carried out in common three electrode cell in which the working electrode was a gold plate (sample E1, A = 0.196 cm^2) with the overoxidized poly(BPA)/PEDOT layer on it in contact with 0.1 mol/dm^3 H_2SO_4 solution, the counter electrode was a ring-shaped Pt plate in the same solution, and the reference electrode was SSCE. Electrochemical impedance measurements were performed right after the overoxidation in 0.1 mol/dm^3 H_2SO_4 solution in the frequency range of 50 kHz–96.1 mHz (amplitude of the perturbing signal: 5 mV rms, electrode potential E = 0.4 V *vs.* SSCE). The cell geometry was the same as described previously. 16 subsequent sets of impedance data were recorded continuously to monitor changes in the polymer film. The start times of the recording of the successive impedance data sequences ("timestamps") were as follows: #1: 0 s, #2: 341.569 s, #3: 683.452 s, #4: 1025.516 s, #5: 1371.936 s, #6: 1718.288 s, #7: 2064.538 s, #8: 2411.373 s, #9: 2754.216 s, #10: 3101.185 s, #11: 3448.118 s, #12: 3795.114 s, #13: 4142.181 s, #14: 4488.584 s, #15: 4839.730 s, #16: 5190.759 s.

Finally, cyclic voltammograms were recorded after the impedance measurements in the potential range of E = –0.4–1.0 V *vs.* SSCE at scan a rate of v = 100 mV/s.

3. Impedance modeling and the calculation of instantaneous impedances

3.1. Impedance modeling

The theory of the impedance of an electrode with diffusion restricted to a thin layer (including conductive polymer films in modified electrodes) is well established, see e.g. [43,45,48–64]. Essentially, two different approaches exist in the literature which are called "homogeneous" ("uniform") [48–57] and "porous medium" (or "heterogeneous") [58–63,65] models, respectively. In [66] a theoretical impedance function for polymer modified electrodes involving coupled diffusion-migration charge transport mechanism with three charge carriers has been derived, which is one of the most general models available in the literature, for which attempts were made to provide a theoretical basis.

In the so called "brush model" introduced earlier [54] it was assumed, that if the cross-sections of the bundles formed by several polymer chains are great enough, their impedance can be described by the equations corresponding to the homogeneous model, or can be well approximated by the expressions derived for the double-channel transmission line model. It should be mentioned that in many cases the mathematical forms of the impedance functions derived for the "homogeneous" and "heterogeneous" models are equivalent, and can be given as [59]:

$$Z_p(\omega) = R_0 + \frac{P_{11}}{s}\coth[Fs] + \frac{P_{12}}{s}\tanh[Fs], \tag{1}$$

where $s = (i\omega)^{1/2}$, (i stands for the imaginary unit, ω is the angular frequency) and the parameters R_0, P_{11}, P_{12} and F are frequency-independent and real. By introducing the thickness of the film L_f, in the simplest cases Eq. (1) can be rewritten as [54,59,66]

$$Z_p(\omega) = R_0 + \frac{P_{11}}{s}\coth\left[\frac{L_f s}{2\sqrt{D^*}}\right] + \frac{P_{12}}{s}\tanh\left[\frac{L_f s}{2\sqrt{D^*}}\right], \tag{2}$$

with a frequency–independent D^*, representing the effective diffusion coefficient of the moving species. It is worth to note here that the different "homogeneous" models have in common that the P_i parameters are inversely proportional to the square route of D^*. On the other hand, most of the models described in the literature predict a so called "Randles circuit behavior" at high frequencies, a Warburg section at intermediate frequencies, and a purely capacitive behavior at low frequencies. Nevertheless, such an "ideal" behavior can seldom be observed in "real" systems. The deviations of the impedance responses from those predicted by the theories have been explained by considering different effects such as interactions between redox sites, ionic relaxation processes, distribution of diffusion coefficients, migration, film swelling, slow reaction with solution species, nonuniform film thickness, inhomogeneous oxidation / reduction processes, experimental artefacts etc. [20,44,60,67].

In the present paper we focus on the impedance modeling of PEDOT or poly(BPA)/PEDOT modified electrodes. It is well known that PEDOT is a good conductor because of its conducting mechanism, and its relation to the doping process [68,69]. These features facilitate modeling, since it can be assumed that simpler models derived for one moving species can be relevant for the description of the impedance response of the system. Such simplified models have been developed and used in several past publications, e.g., in [44,49,55,70–72] as well as in more recent works [73,74]. In accordance with the above studies the expression for the "Faradaic" impedance, when there is only one diffusing species (or in case of electron hopping control or ion movement control) is:

$$Z_p(\omega) = R_{ct} + \frac{P_1}{s}\coth\left[\frac{L_f s}{\sqrt{D^*}}\right] = R_{ct} + Z_d. \tag{3}$$

This differs from the impedance of the "classical" Randles equivalent circuit through the presence of the term $\coth[\frac{L_f s}{\sqrt{D^*}}]$. In Eq. (3) the frequency independent resistive element, R_{ct}, which can be identified as the charge transfer resistance at the metal/polymer interface, is in series with a frequency-dependent impedance element Z_d (sometimes called finite-length transport impedance, or finite-length Warburg impedance). P_1 and L_f are frequency independent and real.

(In connection of the functional form of $Z_p(\omega)$ it is worth mentioning here, that the general formula of the impedance function as a mathematical solution of the problem of diffusion-migration transport of charge carriers within an electrochemically active polymer film in contact with a metal and an electrolyte often takes the form corresponding to Eq. (1), that is, it contains the combination of the hyperbolic functions coth and tanh. Nevertheless, in the special case of $P_{11} = P_{12}$ it can be shown that the sum of the two hyperbolic functions can be effectively replaced by a single coth term like in Eq. (3) (see Appendix A).)

A respective equivalent circuit analog for a polymer modified electrode is shown in Fig. 1.

The equivalent circuit presented in Fig. 1 contains two non-faradaic elements, R_u and Z_{dl}, an uncompensated, frequency independent ohmic resistance (solution resistance) and a capacitive element (double layer capacitance), respectively.

Thus, the overall impedance function of the system is

$$Z(\omega) = Z'(\omega) + iZ''(\omega) = R_u + \frac{1}{1/Z_p(\omega) + 1/Z_{dl}(\omega)} = R_u + \frac{1}{Y_p(\omega) + Y_{dl}(\omega)}, \tag{4}$$

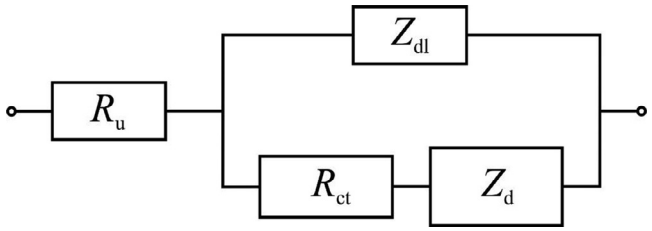

Fig. 1. An equivalent circuit analog for a polymer modified electrode. R_u is an uncompensated, frequency independent ohmic resistance (solution resistance), Z_{dl} is the double layer capacitance, R_{ct} is the charge transfer resistance at the metal/polymer interface, and Z_d is a frequency-dependent impedance element (finite-length Warburg impedance).

where $Z'(\omega)$ and $Z''(\omega)$ are the real and imaginary parts of the impedance, $Y_p(\omega)$ and $Y_{dl}(\omega)$ are the admittances corresponding to $Z_p(\omega)$ and $Z_{dl}(\omega)$, respectively.

In the ideal system

$$Z_{dl}(\omega) = \frac{1}{Y_{dl}(\omega)} = (i\omega C_{dl})^{-1}, \tag{5}$$

where C_{dl} is the (frequency independent) capacitance of the double layer (region) at the gold/polymer film interface.

It should be stressed here that Eq. (3) has been derived for the case of uniform film thickness. However, it is well known that uneven layer thickness is a peculiarity of PEDOT-modified electrodes [17–19]. In the SEM images of PEDOT films deposited on gold (Fig. 2.) well-separated globules (or hierarchical cauliflower-like structures) can be seen on the top of the polymer layer. These structures are highly reproducible and well connected.

This means that any quantitative, or even semi-quantitative information about the morphology of the electrodeposited polymer film can be very helpful in modeling the impedance of the electrodes.

3.1.2. Impedance of the modified electrodes if the thickness of the polymer film is non-uniform

If the thickness of the polymer film is much greater than the thickness of the double layer region at the polymer film/metal interface, it can be assumed that the double layer capacitance and the charge transfer resistance are independent on the thickness and/or the thickness distribution of the polymer layer. This means, that only the thickness dependence of Z_p should be considered in the model.

Without loss of generality, we can assume that the surface of the electrode can be divided into n, not necessarily contiguous segments, each of which is covered by uniform layers of thickness L_i. This means that a discrete-valued distribution (i.e., an empirical frequency distribution) of thickness is used instead of a continuous-valued distribution.

In this case, an approximate impedance function of the system can be expressed as

$$Z(\omega) = R_u + \frac{1}{\frac{1}{Z_{dl}(\omega)} + \sum_{i=1}^{n} \frac{1}{Z_{p,i}(\omega)}} = R_u + \frac{1}{Y_{dl}(\omega) + \sum_{i=1}^{n} Y_{p,i}(\omega)}$$
$$= R_u + \frac{1}{Y_{dl}(\omega) + \sum_{i=1}^{n} x_i \frac{1}{R_{ct,i} + Z_{d,i}(\omega)}}, \tag{6}$$

where x_i is the fraction of the total electrode area covered by a polymer layer of thickness L_i, $Y_{p,i}$ and $Z_{d,i}$ are the faradaic admittance and the finite-length transport impedance, respectively, both corresponding to a uniform layer of thickness L_i. Obviously, $\sum_{i=1}^{n} x_i = 1$.

The equivalent circuit corresponding to Eq. (6) is shown in Fig.3a.

It is worth noting here that based on the above considerations an alternative impedance model can be envisaged in which the charge transfer resistance is completely separated from the transport impedance. In this case, the approximate total impedance takes the following form:

$$Z(\omega) = R_u + \frac{1}{Y_{dl}(\omega) + \sum_{i=1}^{n} Y_{p,i}(\omega)} = R_u + \frac{1}{Y_{dl}(\omega) + \frac{1}{R_{ct} + \frac{1}{\sum_{i=1}^{n} x_i Y_{d,i}(\omega)}}}. \tag{7}$$

The equivalent circuit corresponding to Eq. (7) is shown in Fig. 3b. The equivalent circuits in Fig.3a and b reveal that the differences between the two approximations lie essentially in the possible current routes. Nevertheless, in this study the discussion is limited to the model given by Eq. (6).

3.2. Spline interpolation

As already discussed in the introduction, the successive "impedance diagrams" recorded after overoxidation of the poly(BPA)/PEDOT change continuously with time, it is evident that the system is in a transient state. In such cases a post-experimental analytical procedure is necessary for the reconstruction of "instantaneous impedances". The calculation of the "instantaneous impedances" was carried out using the real and imaginary parts of the impedances measured at identical frequencies („isofrequential components").

For the interpolation procedure a smoothing cubic spline algorithm was used [20,75,76], implemented in LabVIEW. Mathematically, this corresponds to the 4-dimensional analysis proposed by Stoynov [40–42]. As a result a set of instantaneous impedances related to a selected instant of time has been obtained (see Fig. S1 in the supplementary material). The selected time instants correspond to the starting times of the frequency scans. (A free installer package of the software presented at the 71st Annual Meeting of ISE [36] for the correction of "impedance" data measured under non-stationary conditions can be downloaded from the following link: [77].)

3.3. CNLS fitting

Complex non-linear least squares (CNLS) parameter estimations were carried out using the fitting program based on the Levenberg–Marquardt algorithm [76,78,79]. Poisson-weighting was applied in all cases. For checking the goodness-of-fit of the models the four-step procedure [50,53,60,80] has been adopted:

(1) Checking the information about the "mathematical" goodness of the fit, i.e., the statistical analysis of the results of the fitting procedure (sum of squares, variance, correlation matrix, confidence intervals, etc.).
(2) Comparison of impedances calculated by using the estimated (best fit) parameters and the experimental values. A "visual" inspection on both the complex plane plots (Argand diagrams) and the transformed curves (Bode diagrams, complex plane admittance plots, etc.). A model and the estimated parameters can be considered acceptable only if the fit is good in all cases, i.e., for all types of graphical representation of the immittance data.
(3) Analysis of the error structure, i.e., the distribution of the deviations between the measured and calculated (fitted) curves.
(4) The analysis/proofing of the physical significance of the estimated parameters (e.g., dependence of the parameters on different physico-chemical variables, comparison of the estimated values with independent experimental and/or theoretical data, etc.). This step is evidently the most important one in the procedure.

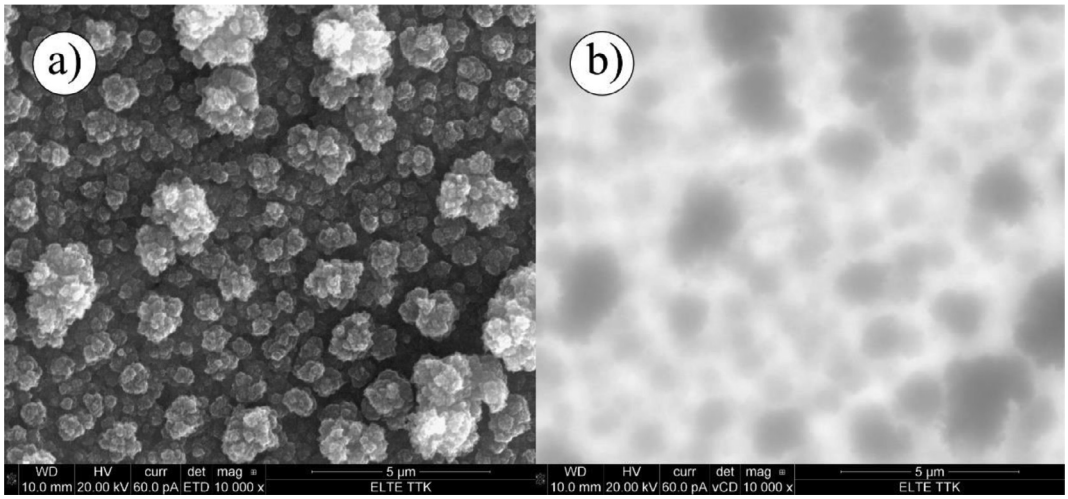

Fig. 2. (a) SEM image of a PEDOT film deposited on Au. (b) The backscattered electron image taken from the same area. The length of the horizontal white bar corresponds to 5 μm.

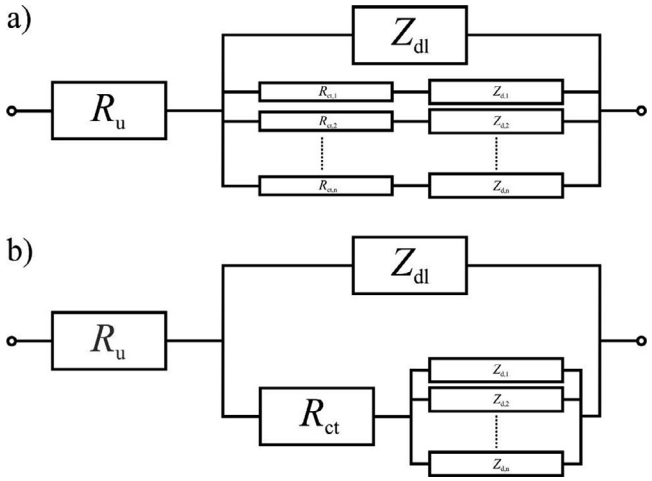

Fig. 3. (a) The equivalent circuit corresponding to Eq. (6). R_u is the uncompensated ohmic resistance, Z_{dl} is the impedance of the double-layer region at the metal/polymer interface. $R_{ct,i}$ is the charge transfer resistance and $Z_{d,i}$ is the finite-length transport impedance which are associated with the polymer layer segment of thickness L_i. (b) The equivalent circuit corresponding to Eq. (7). R_u is the uncompensated ohmic resistance, Z_{dl} is the impedance of the double-layer region at the metal/polymer interface, R_{ct} is the charge transfer resistance at the metal/polymer interface, and $Z_{d,i}$ is the finite-length transport impedance associated with the polymer layer segment of thickness L_i.

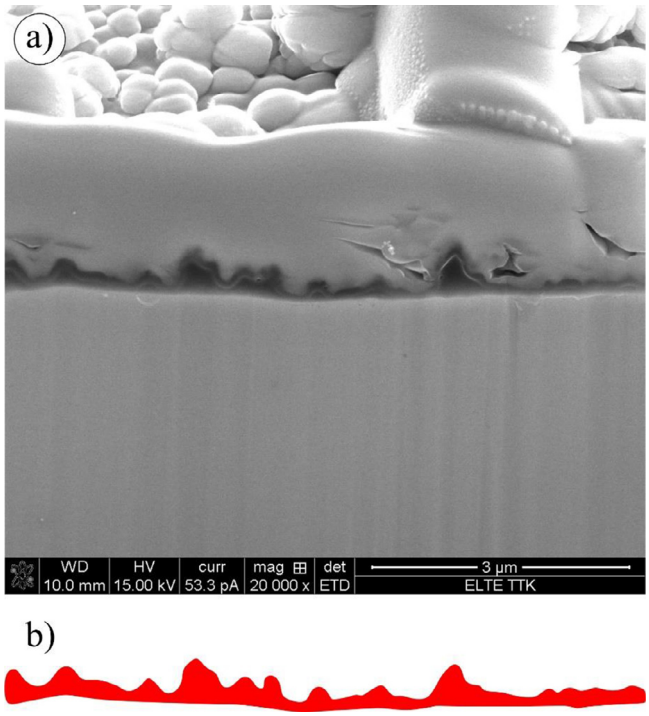

Fig. 4. (a) Focused ion beam (FIB) cross section image of PEDOT film deposited on gold. Deposition time: 1800 s. The length of the horizontal white bar corresponds to 3 μm. (b) "Dark pixels" corresponding to the polymer layer extracted from the SEM micrograph.

4. Results and discussion

4.1. The morphology of the electrochemically deposited PEDOT and poly(BPA)/PEDOT layers

The morphology of the PEDOT layer deposited at a current density of $j = 0.2$ mA/cm^2 for 1800 s was studied by analyzing the scanning electron micrograph shown in Fig. 4. "Dark pixels" (corresponding to the polymer layer) from the SEM micrograph were extracted, and, after horizontal alignment, thickness values were determined by a column-by-column pixel counting and a subsequent scaling based on the image resolution.

For the image presented in Fig. 4 the calculated thicknesses were made subject to a kernel density estimation algorithm [81] that allowed determination of the $p(d)$ probability density function of the d thicknesses in the form of

$$p(d) = \frac{1}{nh}\sum_{i=1}^{n} K\left(\frac{d-d_i}{h}\right). \tag{8}$$

Here n denotes the number of samples in a dataset, and the h bandwidth parameter was estimated by using Silverman's rule of thumb [81] as

$$h = 5\sqrt{\frac{4}{3n}}\sigma, \tag{9}$$

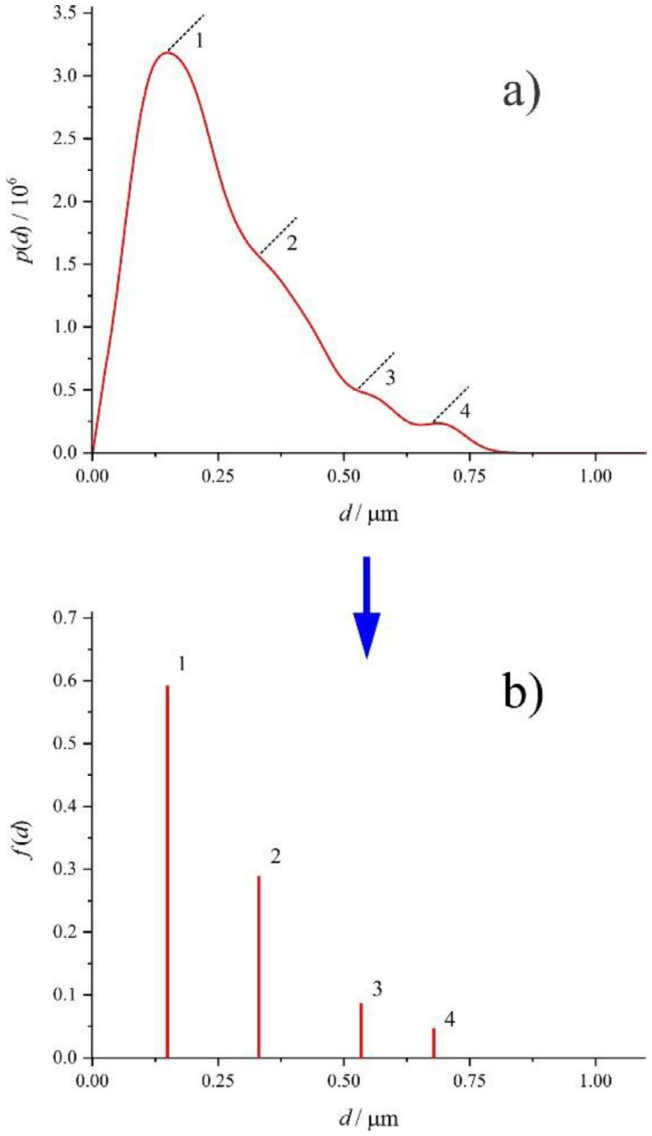

Fig. 5. (a) Estimated function for the thickness distribution of a PEDOT layer deposited on gold. d is the thickness, $p(d)$ is the probability density function d. (b) The 4 characteristic thicknesses. $f(d)$ is the relative frequency of thickness d in the thickness distribution.

where σ is the standard deviation of the sample. For the density estimation a Gaussian kernel defined as

$$K(u) = \frac{1}{\sqrt{2\pi}} \exp\left[-\frac{1}{2}u^2\right] \tag{10}$$

was used.

Estimated function for the thickness distribution of the PEDOT layer deposited on gold is shown in Fig. 5a.

The distribution function in Fig. 5a implies, that 4 characteristic thicknesses can be distinguished in the thickness distribution. Based on this observation, it was expected that the thickness distribution function of the polymer film can be roughly approximated with the distribution of 4 distinct thicknesses, assuming that the surface of the electrode can be divided into 4, not necessarily contiguous segments, each of which is covered with uniform layers (Fig. 5b). In other words, the probability density function of a continuous variable has been replaced by a histogram or a discrete valued probability mass function. In Fig. 5b $f(d)$ is the relative frequency of thickness d in the thickness distribution, which

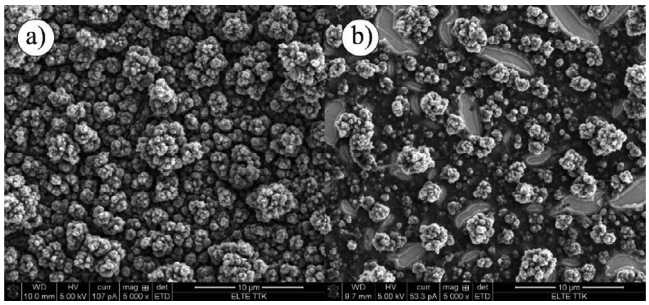

Fig. 6. (a) SEM image of the poly(BPA)-covered PEDOT/Au system. (b) SEM image of the overoxidized poly(BPA)/PEDOT layer on gold. The length of the horizontal white bar corresponds to 10 μm.

corresponds to the surface portion or relative area

$$x_i = \frac{A_i}{A} \tag{11}$$

covered by a film of thickness L_i. (In Eq. (11)) A_i is the area of the electrode covered by the film of thickness L_i, and A is the total area of the electrode.)

A surface structure similar to that of PEDOT (Figs.2 and4) can be seen in Fig. 6a, where the SEM micrograph of the poly(BPA)-covered PEDOT/Au electrode is presented. In the SEM image of the overoxidized poly(BPA)/PEDOT (Fig. 6b) in addition to the cauliflower-like structure cracks or crevices formed during overoxidation [17,19] are clearly visible.

In Fig. 7 focused ion beam (FIB) cross section images taken on the overoxidized poly(BPA)/PEDOT layer (sample E1) are shown.

The following procedure was applied: First, a Pt layer was deposited onto the area of the planned hole to protect and preserve the polymer layer and to avoid Ga contamination (Fig. 7a). The big "cauliflower" like structure with the long filament (what is probably poly(BPA)) in the foreground of Fig. 7a was cut with the Ga ion beam. During the cut, the filament broke away but a piece of it was left behind (Fig. 7b). After that, focused ion beam (FIB) cutting was performed (in the region covered by Pt) to obtain cross sections of the film. The cross-section of the polymer layer can be seen in the SEM image shown in Fig. 7c. As a result, it can be concluded that the thickness distribution of the PEDOT layer is quite similar to that shown is Fig. 4.

4.2. Results of cyclic voltammetry and electro-chemo-mechanical experiments

In Fig.S2a and S2b (presented in the supplementary material) the cyclic voltammograms recorded during the deposition of poly(BPA) on the PEDOT layer (preparation step 3, sample E1) and during overoxidation of the poly(BPA)/PEDOT film (preparation step 5, sample E1) are shown.

Cyclic voltammograms of sample E1 recorded at a sweep rate of $v = 100$ mV s^{-1} in 0.5 M H_2SO_4 solution in the potential range of $E = (-0.1–0.8)$ V vs. SSCE after preparation (step 2), after the deposition of poly(BPA) (step 4), and after overoxidation (recorded after the impedance measurements), respectively, are compared in Fig. 8.

There are some differences between the CVs for Au|PEDOT|0.5 M H_2SO_4 (aq.) and for Au|PEDOT/poly(BPA)|0.5 M H_2SO_4 (aq.) electrodes (curves 1 and 2 in Fig. 8). Although the currents (redox capacities) are practically equal in the potential range of $E = (-0.1–0.1)$ V vs. SSCE, a slight decrease of the current was observed after the deposition of poly(BPA) probably due to a possible (mild) overoxidation of the PEDOT layer. On the other hand, in the voltammogram of the Au|PEDOT/poly(BPA)|0.5 M H_2SO_4 (aq.) electrode a clear oxidation/reduction peak pair can be observed at

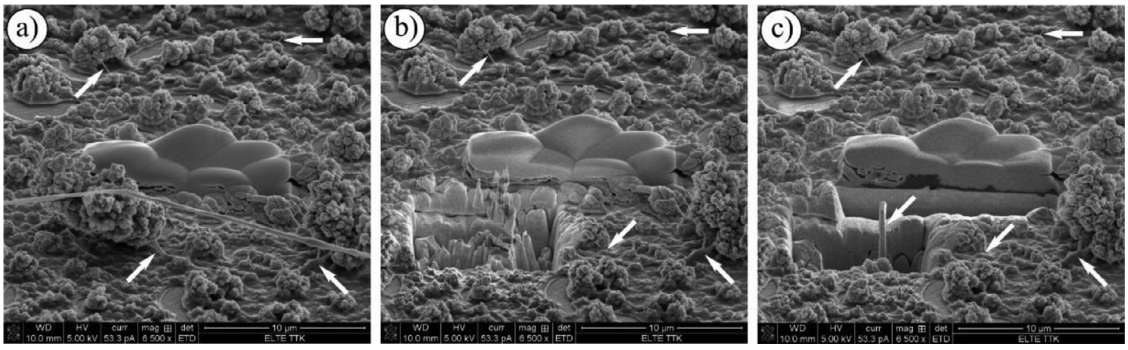

Fig. 7. Focused ion beam (FIB) cross section images (a) before, (b) during and (c) after the cutting process of the overoxidized PEDOT/poly(BPA) layer. The white arrows point to the filaments that presumably belong to the p(BPA) layer. The deposited platinum layer can be seen in the center of the images.

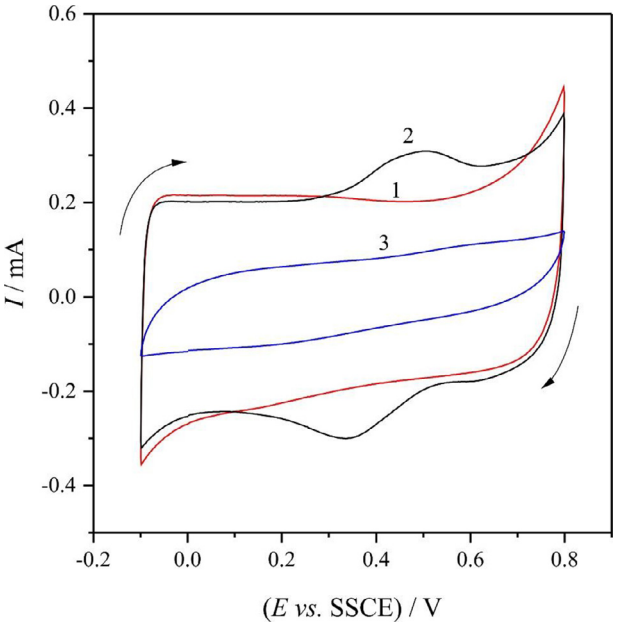

Fig. 8. Cyclic voltammograms of sample E1 (2nd scans) recorded in c = 0.1 mol/dm^3 aqueous H_2SO_4 solution at a sweep rate of v = 100 mV/s in the potential range of E = −0.1–0.8 V *vs.* SSCE: (1) after the preparation of the PEDOT layer, (2) after the deposition of the poly(BPA) layer, (3) after the overoxidation of the PEDOT + PBPA layer and recording the impedance data (16 successive data sets).

about 0.50 V (positive-going potential scan) and 0.33 V (negative-going potential scan), respectively (curve 2 in Fig. 8). This redox peak pair practically disappears during overoxidation of the poly(BPA)/PEDOT film (see curve 3 in Fig. 8).

In case of sample F1 (A = 0.196 cm^2, 0.01 mol/dm^3 EDOT / 0.1 mol/dm^3 Na_2SO_4 solution, deposition time: t = 600 s, current density: j = 0.2 mA/cm^2), the oxidation/reduction peak pair in the voltammogram of the Au|PEDOT/poly(BPA)|0.5 M H_2SO_4 (aq.) electrode appears at about 0.5 V and 0.4 V vs. SSCE, respectively, however the redox peak pair does not disappear completely during the overoxidation process, but the potential maximum of the reduction peak shifts in the negative direction to about 0.34 V vs. SSCE (see curves 2 and 3 in Fig. S3).

As it can be seen in Figs.8 and S3, after overoxidation of the poly(BPA)/PEDOT layer the redox capacities of the modified electrodes (i.e., the currents in the cyclic voltammograms) are always considerably smaller than those of the freshly prepared films. This observation is also true for the electrodes containing layers of "pure" PEDOT. Cyclic voltammograms of sample F3 recorded after deposition of the PEDOT film (step 1) and after overoxidation of the polymer (using cyclic voltammetry: 3 potential cycles in the potential range up to 1.5 V vs. SSCE) are presented in Fig. S4. By comparing Figs.S4 (curve 2) and Fig. S3 (curve 3) it can be clearly seen that at the same level of overoxidation the CV currents (i.e., the absolute values of the positive and negative currents) measured for the overoxidized PEDOT modified electrode are considerably lower than those measured in the case of overoxidized poly(BPA)/PEDOT. One plausible reason for this can be identified by a simple visual inspection of the PEDOT and poly(BPA)/PEDOT layers after intensive overoxidation. The photographs in Fig. 9 were taken after dipping samples F1 and F3 into ultrapure water multiple times. It can be well seen that a significant part of the overoxidized PEDOT layer has been detached from the gold substrate, while the overoxidized poly(BPA)/PEDOT layer has remained more or less intact.

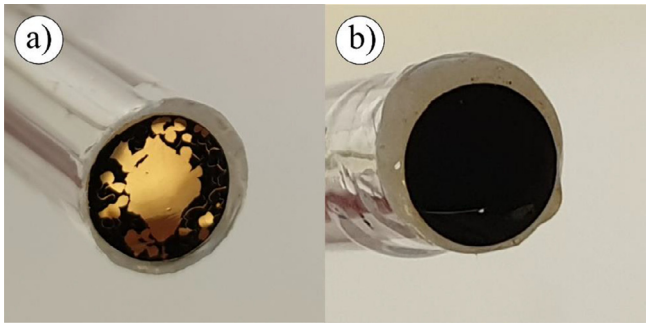

Fig. 9. Photographs of samples F1 and F3 after (strong) overoxidation. (a) the "pure" PEDOT layer (sample F3), (b) the PEDOT + poly(BPA) layer (sample F1).

In order to justify the above observations, we have carried out some preliminary experiments to obtain some quantitative data on the changes in the mechanical properties of the polymer layers due to overoxidation. It is well known that measuring the bending of a plate or strip to determine interface stress change or the stress in thin films is a quite frequently used technique in electrochemistry [25,82–84]. In our present experiments, we used the experimental setup reported e.g. in [16,17,85–87] and cantilever electrodes covered by PEDOT and PEDOT+poly(BPA) films corresponding to those of samples E1–E3. A concise description of the experimental apparatus, the measurement technique, and the data used in the calculations can be found in the supplementary material (section "Stress change measurements").

The results of the stress change measurements in the potential range from –0.1 V–0.8 V vs. SSCE show that in case of the Au|PEDOT|0.1 M sulfuric acid electrode the difference between the minimum and maximum values of the change in the film stress ($\Delta\Delta g_f$) is about 4.3 MPa, while for the Au|PEDOT+poly(BPA)|0.1 M sulfuric acid electrode the corresponding value is about 3.2 MPa. The observed difference can be at least partly attributed to the

mild overoxidation of the PEDOT film during the deposition of poly(BPA). Both voltdeflectograms (the change of the curvature of the strip, $\Delta(1/R)$, with respect to the electrode potential, E) show pronounced hysteresis implying that stress changes in the polymer films may significantly contribute to the changes in $1/R$ (see Fig. S5b, curves 1 and 2). The cyclic voltammogram recorded for the Au|PEDOT+poly(BPA)|0.1 M sulfuric acid electrode after overoxidation (Fig. S5c, curve 4) is similar to the CV of the Au|PEDOT|0. M sulfuric acid electrode (Fig. S5c, curve 3) in shape, but the charging currents are somewhat smaller in the latter case. On the other hand, as it can be well seen in Fig. 5b that the shapes of the $\Delta(1/R)$ vs. E curves change considerably as a result of overoxidation. After the application of 3 potential cycles up to 1.45 V vs. SSCE, in case of the Au|PEDOT+poly(BPA)|0.1 M sulfuric acid electrode the difference between the minimum and maximum values of $\Delta(1/R)$ is about 0.0015 m^{-1} (Fig. S5b, curve 4). This corresponds to $\Delta\Delta g_f \approx 1.1$ MPa, indicating some remaining electro-chemo-mechanical activity of the residual polymer layer. In contrary to this, in case of the Au|PEDOT|0.1 M sulfuric acid electrode the difference is less than 0.0006 m^{-1} (curve 3 in Fig. S5b) corresponding only to about 0.4 MPa. These results are in line with the (qualitative) finding that the poly(BPA) supported PEDOT film is mechanically more resistant to the effects of overoxidation than the "pure" PEDOT film.

It should be stressed here, that the original bending beam theory treats the thin layer on the substrate as a uniform material. It is well known, however, that polymer films have complex internal structure. Although in some polymer/metal systems the polymer film completely blocks the metal surface, but this is not always the case. For example, if pores are present in the film, the electrolyte solution may contact the underlying metal layer at the bottom of the pores, and the change in the surface stress of the metal/solution interface with electrode potential occurs simultaneously with the change of the film stress. Both processes can result in a change in the radius of curvature (R) of the strip. The contributions from surface and bulk cannot be separated in the general case, and the exact values of the film stress changes remain uncertain. (Therefore, we show only the "voltdeflectograms", i.e. the $\Delta(1/R)$ vs. E plots in Fig. S5b.) Nevertheless, the results of the bending beam experiments can be used quite effectively to compare the electro-chemo-mechanical properties of similar systems.

4.3. Impedance measurements

4.3.1. Impedance of the modified electrodes before overoxidation

In Fig. 10 results of impedance measurements in different representations are plotted (complex plane impedance plots, Bode plots, capacitance $C_p = (Y''/\omega)$ vs. log(frequency) plots, and complex plane admittance plots). The impedance spectra shown in Fig. 10 were recorded for the Au|PEDOT|0.1 M H_2SO_4(aq.) and Au|PEDOT/poly(BPA)|0.1 M H_2SO_4(aq.) electrodes (sample E1), i.e. before and after the deposition of poly(BPA), respectively, in the frequency range of 50 kHz–96.1 mHz, at the electrode potential $E = 0.4$ V vs. SSCE. The excitation signal was 5 mV (rms).

As it can be seen in Fig. 10a the impedance response of the Au|PEDOT|0.1 M H_2SO_4(aq.) electrode at medium and low frequencies (Fig. 10a and d, curve 1) is similar to that of a pure capacitor (near –90 ° phase angle). On the other hand, the Au|PEDOT/poly(BPA)|0.1 M H_2SO_4(aq.) electrode shows at low frequencies a pattern characteristic for a constant phase element (CPE) with an exponent different from unity (Fig. 10a and d, curve 2). The impedance vs. angular frequency function of a CPE is given as

$$Z(\omega) = (\mathrm{i}\omega T)^{-\theta} = \frac{1}{T^*}(\mathrm{i}\omega)^{-\theta}, \tag{12}$$

where $\theta \leq 1$, but in the above discussed case θ is usually close to 1. This behavior can be attributed e.g. to the presence of the poly(BPA) layer on the PEDOT film and/or to the mild overoxidation of the PEDOT film during the electrochemical deposition of poly(BPA). At higher frequencies an arc can be identified in both cases (see Fig. 10a, insert).

4.3.2. 2 Adaptation of Eq.(6) to the specific conditions

Based on what we already know about these electrodes we tried to find a suitable impedance model for data analysis. Starting with the results of the morphological investigations (Section 4.1.) and based on the considerations concerning the impedance of modified electrodes if the thickness of the polymer layer is not uniform (Section 3.1.2.), we can assume that the surface of the electrode can be divided into 4 non-overlapping, but not necessarily contiguous regions or segments of uniform thicknesses, and the layer thicknesses in the different regions are different. In this special case the overall impedance function of the system (see Eq. (6)) can be expressed as

$$\begin{aligned} Z(\omega) &= R_u + \frac{1}{Y_{dl}(\omega) + \sum_{i=1}^{n} Y_{p,i}(\omega)} \\ &= R_u + \frac{1}{Y_{dl}(\omega) + \sum_{i=1}^{4} x_i \frac{1}{R_{ct,i} + Z_{d,i}(\omega)}}. \end{aligned} \tag{13}$$

Obviously, $x_1 + x_2 + x_3 + x_4 = 1$.

It should be noted here that we can measure the film thickness in the dry state, and an estimation can be made for the thickness distribution. However, due to the swelling of the polymer film the thicknesses determined in the dry state give only qualitative information about the real thickness of the film in contact with an electrolyte solution, especially in the charged state. Nevertheless, it is a plausible assumption that the characteristics of the thickness distributions are very similar in the two cases, and overoxidation does not change this either.

If we also assume that P_1 and D^* in Eq. (3) and the charge transfer resistances ($R_{ct,i}$) in Eq. (13) are independent of the local thickness of the polymer film, Eq. (13) can be rewritten as

$$Z(\omega) = R_u + \frac{1}{Y_{dl}(\omega) + \sum_{i=1}^{4} x_i \frac{1}{R_{ct} + \frac{P_1}{s}\coth\left[\frac{L_i s}{\sqrt{D^*}}\right]}}, \tag{14}$$

or more detailed:

$$Z(\omega) = R_u + \frac{1}{Y_{dl}(\omega) + \sum_{i=1}^{3} \frac{x_i}{R_{ct} + \frac{P_1}{s}\coth\left[\frac{L_i s}{\sqrt{D^*}}\right]} + \frac{1 - x_1 - x_2 - x_3}{R_{ct} + \frac{P_1}{s}\coth\left[\frac{L_4 s}{\sqrt{D^*}}\right]}} \tag{15}$$

If the capacitance of the double layer region at the gold/polymer interface (C_{dl}) does not depend on the frequency, then Eq. (15) takes the form:

$$Z(\omega) = R_u + \frac{1}{\mathrm{i}\omega C_{dl} + \sum_{i=1}^{3} \frac{x_i}{R_{ct} + \frac{P_1}{s}\coth\left[\frac{L_i s}{\sqrt{D^*}}\right]} + \frac{1 - x_1 - x_2 - x_3}{R_{ct} + \frac{P_1}{s}\coth\left[\frac{L_4 s}{\sqrt{D^*}}\right]}}. \tag{16}$$

According to Eq. (16), a constant, frequency-independent capacitance (C_L) should be observed at low frequencies (see Appendix B). However, in contrast to this, the low-frequency parts of the impedance spectra recorded for the Au|PEDOT|0.1 M H_2SO_4(aq.) and Au|PEDOT/poly(BPA)|0.1 M H_2SO_4(aq.) electrodes are very similar to the impedance responses characteristic for constant phase elements with exponents slightly less than unity (see

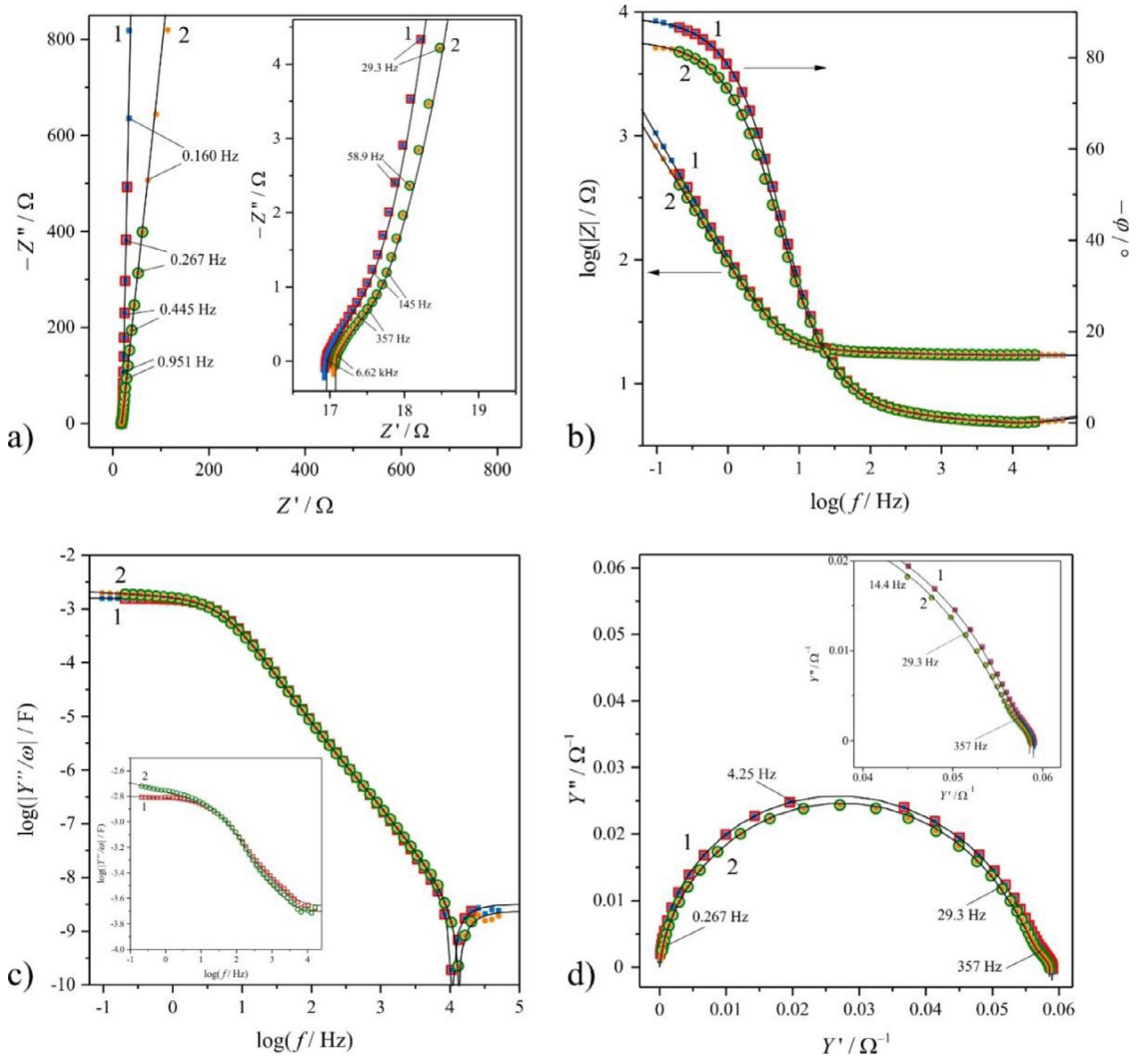

Fig. 10. The results of the impedance measurements on the Au|PEDOT|0.1 M H_2SO_4(aq.) (1) and Au|PEDOT/poly(BPA)|0.1 M H_2SO_4(aq.) (2) electrodes in different representations (sample E1 before and after the deposition of poly(BPA)): (a) Complex plane impedance plots (Z' is the real part and Z'' is the imaginary part of the complex impedance), the high frequency regions are shown in the insert, small numbers in the plots refer to frequency values; (b) Bode plots (logarithm of the magnitude (log|Z|) and the phase angle (φ) vs. the logarithm of the frequency (log f));(c) Logarithm of the absolute value of Y'' / ω (the imaginary part of the admittance divided by the angular frequency, sometimes called the "parallel capacitance" of the electrode) as a function of the logarithm of the frequency (log(|Y'' / ω| vs. log f), the same data corrected by the estimated ohmic resistance (R_u) are shown in the insert, small numbers in the plots refer to frequency values; (d) Complex admittance plane plots (imaginary part of the admittance (Y'') versus the real part of the admittance (Y')), the high frequency regions are shown in the insert. The impedances data were measured at the electrode potential of E = 0.4 V vs. SSCE, in the frequency range of 50 kHz–96.1 mHz. The amplitude of the perturbing signal was 5 mV. The data points are indicated by "full" symbols, (1): ■ and (2): ●. The solid curves were calculated (simulated) by using the "best-fit" parameters given in Table 1. The impedance data in the 20.4 kHz – 207 mHz frequency range were fitted. The data points used in the CNLS fitting process are indicated by "empty" symbols, (1): □ and (2): ○.

Eq. (12)). On the other hand, well-defined but slightly depressed arcs can be identified in the complex plane plots at higher frequencies. Therefore, in order to obtain an impedance expression which fits the experimental data better [53,66], the theoretical expression has been modified heuristically by introducing a constant phase element (CPE) to describe the immittance of the substrate/polymer interfacial region (see also Eqs.(5) and (12)):

$$Z_{dl}(\omega) = (i\omega B)^{-b} \tag{17}$$

In this case instead of Eq. (16), the following equation can be used in the parameter estimation procedure:

$$Z(\omega) = R_u + \frac{1}{(i\omega B)^b + \sum_{i=1}^{4} x_i \frac{1}{R_{ct} + \frac{P_1}{s} \coth\left[\frac{L_i s}{\sqrt{D^*}}\right]}}. \tag{18}$$

The introduction of the new parameter b is only acceptable when the optimized value of b is not much smaller than 1 (see Eq. (12)). In addition, it is well known that the effect of inductance is especially significant for circuits with low impedances. It can be clearly seen in Fig. 10a (insert) that this is precisely the case here. The inductive impedance is most probably caused by the connector cables (wiring), since even a straight piece of wire has a small but measurable self inductance (L). This means that the expression has to be completed by adding the term

$$Z_L(\omega) = i\omega L \tag{19}$$

in series to represent the inductive impedance behavior. This means that

$$Z(\omega) = i\omega L + R_u + \frac{1}{(i\omega B)^b + \sum_{i=1}^{4} x_i \frac{1}{R_{ct} + \frac{P_1}{s} \coth\left[\frac{L_i s}{\sqrt{D^*}}\right]}}. \tag{20}$$

In Eq. (19) L, R_u, R_{ct}, B, b, x_1, x_2, x_3, P_1, D^*, L_1, L_2, L_3, and L_4 are frequency independent and real. Unfortunately, the fitting in the case of such a high number of parameters is always a very difficult task. In addition, due to the mathematical structure of Eq. (20), the

Table 1
Results of CNLS fitting of impedance data obtained for the Au|PEDOT|0.1 M H_2SO_4(aq.) and Au|PEDOT/poly(BPA)|0.1 M H_2SO_4(aq.) electrodes (sample E1) before overoxidation (estimated mean values and standard errors). The electrochemical impedance measurements were performed in the frequency range of 20.4 kHz to 207 mHz, amplitude of the perturbing signal: 5 mV rms, electrode potential $E = 0.4$ V *vs.* SSCE. L: inductance, R_u: uncompensated ohmic resistance (solution resistance), R_{ct}: the charge transfer resistance at the metal/polymer interface, B and b: parameters of the constant phase element (B can be regarded as the approximate value of the capacitance of the double layer region, P_1: parameter of the finite-length transport impedance, F_i: parameters corresponding to $L_i\ /(D^*)^{1/2}$ (L_i: layer thickness of region i, D^*: effective diffusion coefficient of the moving species), x_i: the fraction of the total electrode area covered by a polymer layer of thickness L_i.

	Au|PEDOT|0.1 M H_2SO_4 (aq.)		Au|PEDOT/poly(BPA)|0.1 M H_2SO_4 (aq.)	
degrees of freedom	37		37	
weighted sum of squares (Q)	$1.54020\cdot\cdot10^{-1}$		$1.36674\cdot10^{-1}$	
weighted standard error	$4.16271\cdot10^{-3}$		$3.69388\cdot10^{-3}$	
Parameter	estimated value	standard error	estimated Value	Standard error
L / H	$9.567990\cdot10^{-7}$	$1.291090\cdot10^{-7}$	$8.521437\cdot10^{-7}$	$1.267654\cdot10^{-7}$
R_u / Ω	16.94284	$5.440365\cdot10^{-2}$	17.05140	$4.819549\cdot10^{-2}$
R_{ct} / Ω	$2.391469\cdot10^{-2}$	$(1.912878)^*$	$4.566461\cdot10^{-2}$	$(2.661143\cdot10^{-1})^*$
B / $F\cdot\Omega^{1-1/b}$	$1.920205\cdot10^{-4}$	$(6.659594\cdot10^{-4})^*$	$1.691200\cdot10^{-4}$	$7.108548\cdot10^{-5}$
Bb	$9.366462\cdot10^{-1}$	$1.337212\cdot10^{-1}$	$8.217659\cdot10^{-1}$	$2.475208\cdot10^{-2}$
P_1 / $\Omega\cdot s^{-1}$	55.10507	7.604196	62.90910	9.372214
F_1 / $s^{1/2}$	$2.677074\cdot10^{-1}$	$1.697638\cdot10^{-1}$	$2.368964\cdot10^{-1}$	$9.222801\cdot10^{-2}$
F_2 / $s^{1/2}$	$1.421732\cdot10^{-1}$	$6.807794\cdot10^{-2}$	$5.695281\cdot10^{-2}$	$1.301238\cdot10^{-2}$
F_3 / $s^{1/2}$	$2.522524\cdot10^{-2}$	$(6.807794\cdot10^{-2})^*$	$2.437433\cdot10^{-2}$	$(3.847408\cdot10^{-2})^*$
F_4 / $s^{1/2}$	$6.231921\cdot10^{-2}$	$3.888597\cdot10^{-2}$	$1.299026\cdot10^{-1}$	$5.542458\cdot10^{-2}$
x_1	$1.980080\cdot10^{-2}$	$(4.479857\cdot10^{-2})^*$	$4.618395\cdot10^{-2}$	$(7.718645\cdot10^{-2})^*$
x_2	$1.533732\cdot10^{-1}$	$6.719340\cdot10^{-2}$	$6.748237\cdot10^{-1}$	$1.413855\cdot10^{-1}$
x_3	$2.677470\cdot10^{-1}$	$1.450069\cdot10^{-1}$	$1.026513\cdot10^{-1}$	$(1.867130\cdot10^{-1})^*$
$1-x_1-x_2-x_3$	$5.59079\cdot10^{-1}$	-	$1.7634105\cdot10^{-1}$	-

* : poorly determined

parameters are expected to be strongly correlated. For example, by inspecting Eq. (20) we can immediately see that L_1, L_2, L_3, L_4 and D^* cannot be determined separately by CNLS fitting, only the

$$F_i = \frac{L_i}{\sqrt{D^*}} \tag{21}$$

values can be obtained by fitting Eq. (20) to the experimental data. By introducing the variables F_1, F_2, F_3 and F_4 into Eq. (20) the expression of the overall impedance takes the following form:

$$Z(\omega) = \mathrm{i}\omega L + R_u + \frac{1}{(\mathrm{i}\omega B)^b + \sum_{i=1}^{4} x_i \frac{1}{R_{ct}+\frac{P_1}{s}\coth[F_i s]}}. \tag{22}$$

4.3.3. Results of the parameter estimation for the modified electrodes before overoxidation

Indeed, in respect of the statistical information one cannot expect too much from a fitting procedure with 13 free parameters. Nevertheless, we tried to use Eq. (22) (as a model/objective function) for parameter estimation. Impedances measured in the frequency range of 20.4 kHz to 207 mHz were fitted using the Marquardt least squares algorithm [76,78,79]. Statistically, the fitting results were not satisfactory in all respects. While we could obtain well defined mean values of the parameter estimates ("best-fit" parameters), we observed that several parameters are strongly correlated, and the method did not yield reliable confidence intervals for them. (The mean values of the parameter estimates for both the Au|PEDOT|0.1 M H_2SO_4(aq.) and Au|PEDOT/poly(BPA)|0.1 M H_2SO_4(aq.) electrodes are listed in Table 1.) On the other hand, however, despite the uncertainties of the parameter estimation, the visual inspection of the fitted curves and the original data presented in Fig. 10 suggests that the model fits the observed data quite well (and this holds true for all relevant representations considered in the present study (Bode plot, complex admittance plot, (Y''/ω) vs. log f plot)). The curves calculated by using the best-fit parameters (represented by the solid lines in Fig. 10) fit the measured data reasonably well even outside the frequency range used for parameter estimation (from 50 kHz down to 96.1 mHz), asserting that the parameter estimation is robust in this regard. In addition, the values of all fitting parameters appear physically reasonable. (This points up the fallacy of evaluating the 'goodness' of a result in terms of statistical significance alone.)

In addition to the aspects discussed above, the investigation of the deviation between the measured and the best fit simulated curves can provide information in respect of the nature (systematic or random) of the fitting errors. In the case of unweighted data, a "good" fit the deviations show a normal (Gaussian-like) distribution. In the case of weighted data, one can usually be satisfied if the deviations do not show a systematic trend. This can best be determined by plotting the real and imaginary components of the deviations against each other ("scatter plot"). Based on the visual inspection of the plots in Fig. 11 we may arrive at the conclusion, that the results of the parameter estimation procedures are acceptable in both cases, although in Fig. 11b some faint trend can be identified in the diagrams.

4.3.4. Impedance of the Au|PEDOT/poly(BPA)|0.1 M H_2SO_4(aq.) electrode after overoxidation

As described in the experimental section, subsequent impedance measurements were performed on the strongly overoxidized Au|PEDOT/poly(BPA)|0.1 M H_2SO_4(aq.) electrode at the electrode potential of $E = 0.4$ V vs. SSCE in the a frequency range of 50 kHz–96.1 mHz (see step 6 in Section 2.3.). The impedance measurements started immediately after the last overoxidation cycle, and this time instant was chosen as the starting time of the impedance measurements ("timestamp": $t = 0$ s). 16 successive impedance spectra were recorded. The recording time of a "single" spectrum was about 342 s. The complex plane diagrams in Fig. 12 are similar to those reported for other polymer modified electrodes, including electrodes with overoxidized PEDOT films [19–22,50,60]. The impedance data show a capacitive arc in the high-frequency region and a capacitive domain at low frequencies. Only a narrow Warburg-like region (if any) can be observed between the high-frequency arc and the low frequency sloped line.

As it can be seen in Fig. 12, the impedance data sets recorded successively after overoxidation of the poly(BPA)/PEDOT change continuously with time, it is evident that the system is in a transient state. In principle, in such cases corrections are necessary

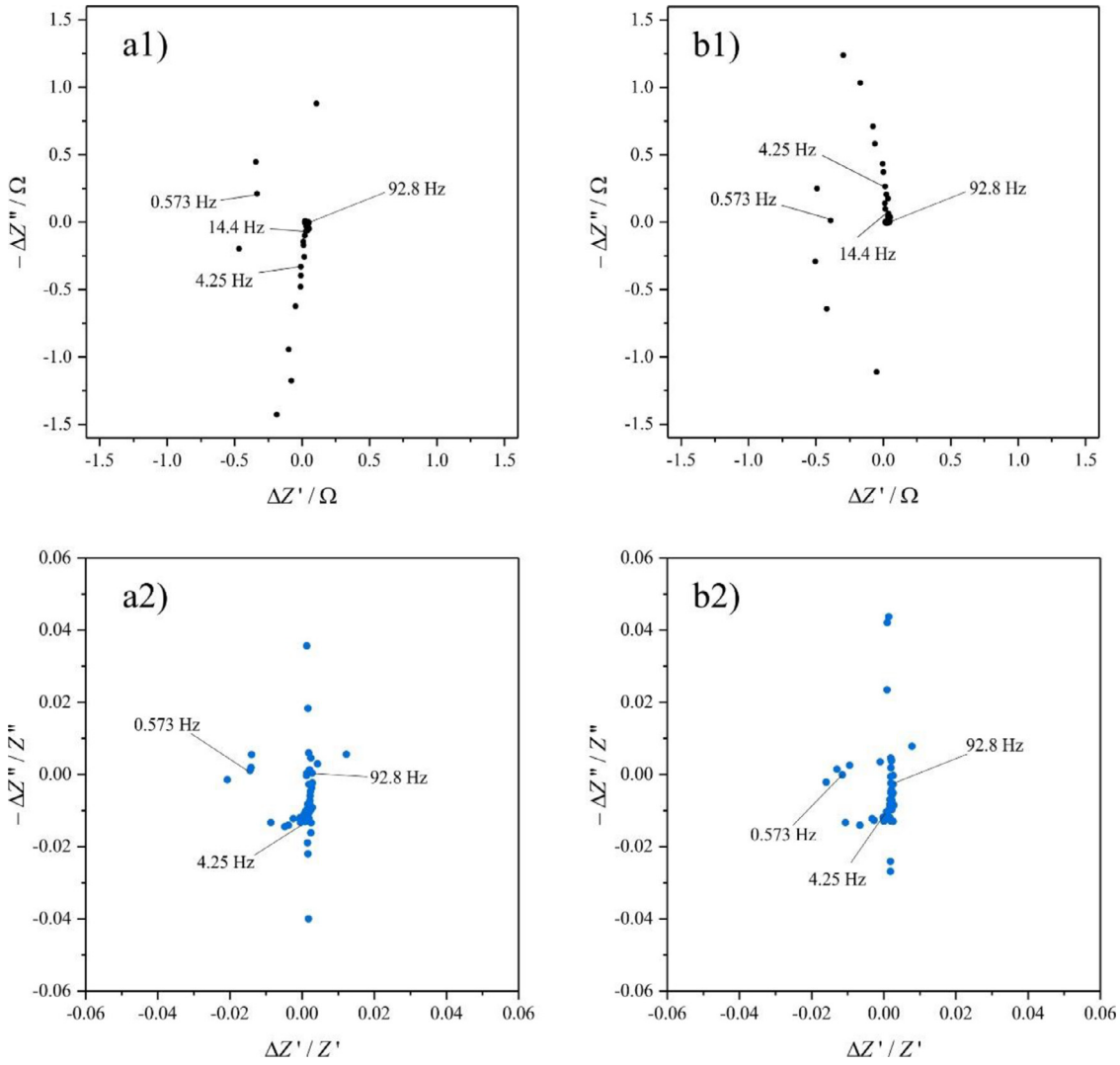

Fig. 11. Absolute (a1 and b1) and relative (a2 and b2) deviations of the measured and the best fit data in the complex plane. (The measured and fitted data for sample E1 are presented in Fig. 10). (a1) and (a2) Au|PEDOT|0.1 M H_2SO_4(aq.) electrode, (b1) and (b2) Au|PEDOT/poly(BPA)|0.1 M H_2SO_4(aq.) electrode, respectively.

to obtain true impedance spectra suitable for parameter estimation based on model impedance functions. As already discussed in Section 3.2, the calculation of the "instantaneous impedances" was carried out using the real and imaginary parts of the impedances measured at identical frequencies („isofrequential components"). The diagrams in Fig. 13 show selected sets of experimental data points measured during the frequency sweeps, each of which started at a given time t_i (see also Table S1 in the supplementary material), together with the corresponding calculated impedance spectra. According to Fig. 13 the differences between the measured and corrected/calculated impedance values are quite small at high frequencies but are more significant in the low-frequency range.

To investigate the implications of the FDA corrections on the values of the estimated parameters, parameter estimations were carried out using both the uncorrected and corrected impedance data sets. The impedance data measured in the frequency range from $f = 96.1$ mHz to $f = 10.378$ kHz were used for parameter estimation. As it has already been discussed, the "direct" application of Eq. (22) in a parameter estimation procedure encounters problems due to the high number of correlated variables. Nevertheless, Eq. (22) can be simplified by omitting the $i\omega L$ term, since it is expected that $L < 10^{-6}$ H (see Table 1), and the contribution of the parasitic inductances to the total impedance is less than 0.07 Ω. Another possibility to further reduce the number of the free parameters is to fix the values of some of the correlated parameters using a priori information and then optimize the remaining values. It is well known that models with many free parameters (like Eq. (22)) can often have significant parameter degeneracies, making the correlation matrix obtained from the parameter estimation procedure a valuable tool for evaluating the specific model parameterization. Absolute values of correlation coefficients close to unity indicate significant degeneracies ($|c_{jk}| = 1$ can be interpreted as perfect synchrony) which can prevent the minimization algorithm from efficiently and accurately converging [88]. From the correlation matrices it can be concluded that there are strong correlations between the parameters x_1 – x_3 and F_1 – F_4. Therefore, knowing that in Eq. (22) the parameters x_1 – x_4 represent the fractions of the total electrode area covered with layers of different thicknesses, we tried to estimate the empirical distribution of the x_i values (this clearly differs from that before overoxidation). Several attempts were made to find the best combination, the only (arbitrary) assumption was that the distribution is independent of time. The lowest values of the objective functions were attained by using the following values: $x_1 = x_3 = 0.25$, $x_2 = 0.30$. These results match quite well with those

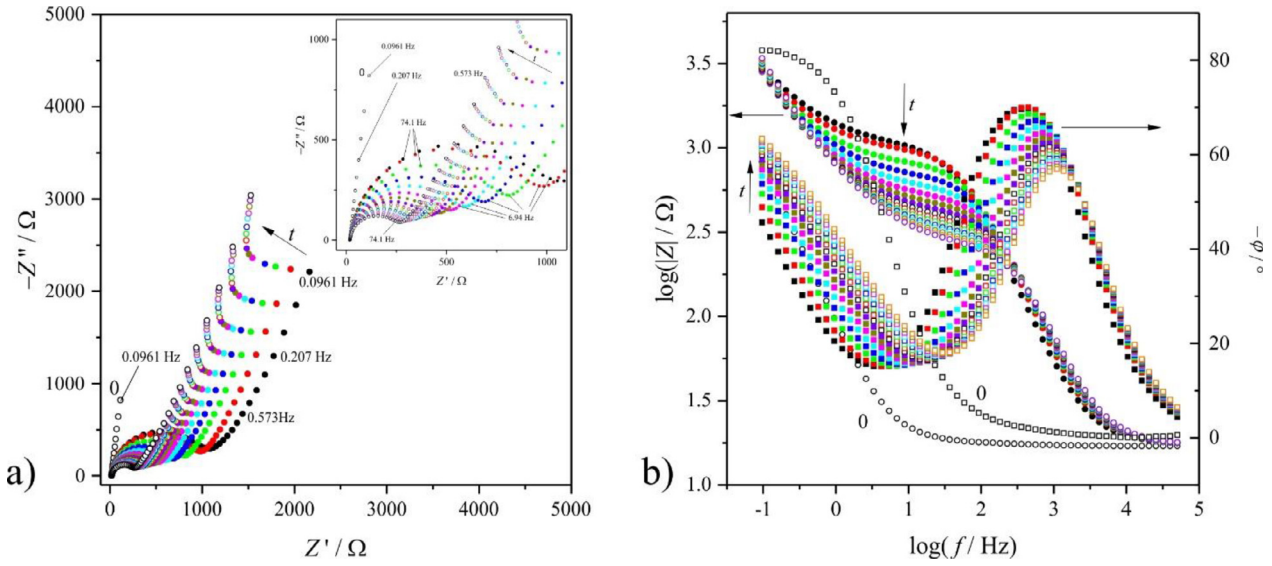

Fig. 12. Impedance data sets recorded before (0) and subsequently after overoxidation (t) on the Au|PEDOT/poly(BPA)|0.1 M H_2SO_4(aq.) at electrode potential E = 0.4 V vs. SSCE, and in the frequency range f = 50 kHz–96.1 mHz. The start times of the recording of the successive impedance data sequences ("timestamps") were as follows: #1: 0 s, #2: 341.569 s, #3: 683.452 s, #4: 1025.516 s, #5: 1371.936 s, #6: 1718.288 s, #7: 2064.538 s, #8: 2411.373 s, #9: 2754.216 s, #10: 3101.185 s, #11: 3448.118 s, #12: 3795.114 s, #13: 4142.181 s, #14: 4488.584 s, #15: 4839.730 s, #16: 5190.759 s. (a) Complex impedance plane plots (imaginary part of the impedance (Z '') vs. the real part (Z ') of the impedance), the high frequency regions are shown in the insert. Small numbers in the plots refer to frequency values; (b) Bode plots (the logarithm of magnitude (log|Z| or the phase angle (φ) vs. logarithm of the frequency (log f)).

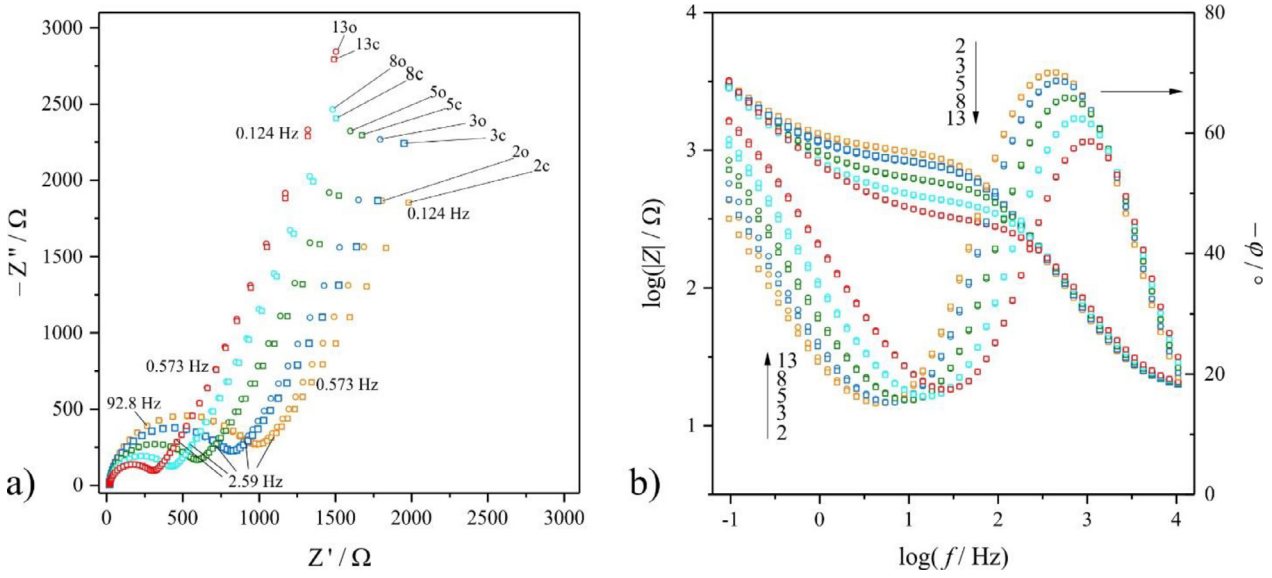

Fig. 13. Comparison of directly measured ("original") impedance data sets (○, 2o–5o, 8o, 13o) and calculated ("instantaneous") impedance spectra (□, 2c–5c, 8c, 13c) recorded for the Au|PEDOT/poly(BPA)|0.1 M H_2SO_4(aq.) electrode (sample E1) at the electrode potential E = 0.4 V vs. SSCE in the frequency range of f = 50 kHz–96.1 mHz after the overoxidation of the film. (a) Complex impedance plane plot (Z ' is the real part and Z '' is the imaginary part of the complex impedance). Small numbers in the plots refer to frequency values; (b) Bode plots (logarithm of the magnitude (log|Z|) and the phase angle (φ) vs. the logarithm of the frequency (log f)).

estimated by visual inspection of the SEM images taken on dry samples.

After the above simplifications (and by neglecting the contribution of the cracks and other uncovered segments of the substrate to the overall electrode impedance) the model function used for fitting can be written as:

$$Z(\omega) = R_u + \frac{1}{(i\omega B)^b + \sum_{i=1}^{4} \hat{x}_i \frac{1}{R_{ct} + \frac{P_1}{s} \coth[F_i s]}}. \quad (23)$$

where the $\hat{x}_i$-s are fixed (see above), and the adjustable parameters are: R_u, R_{ct}, B, b, P_1, F_1, F_2, F_3, and F_4. The results of the fitting (including mean values of the estimated parameters, standard deviations, and confidence intervals at the 95% confidence level) are summarized in Table S1 in the supplementary material. As it can be seen from Table S1, despite the still high number of the parameters, most of them could be determined with good statistics, and reasonable estimated mean values have been obtained for all of them. And this is, somewhat surprisingly, true for all data sets, including the directly measured impedances and the impedance spectra calculated by using the 4-dimensional analysis method [20,21,39–42]. In addition, as it can be seen in Figs. 14 and 15, the curves (impedance spectra) simulated by using the mean values of the estimated parameters closely fit the measured data, and this holds for both the complex plane impedance plots and the transformed data representations (Bode plots, complex plane admittance plot, C_p vs. log f plot).

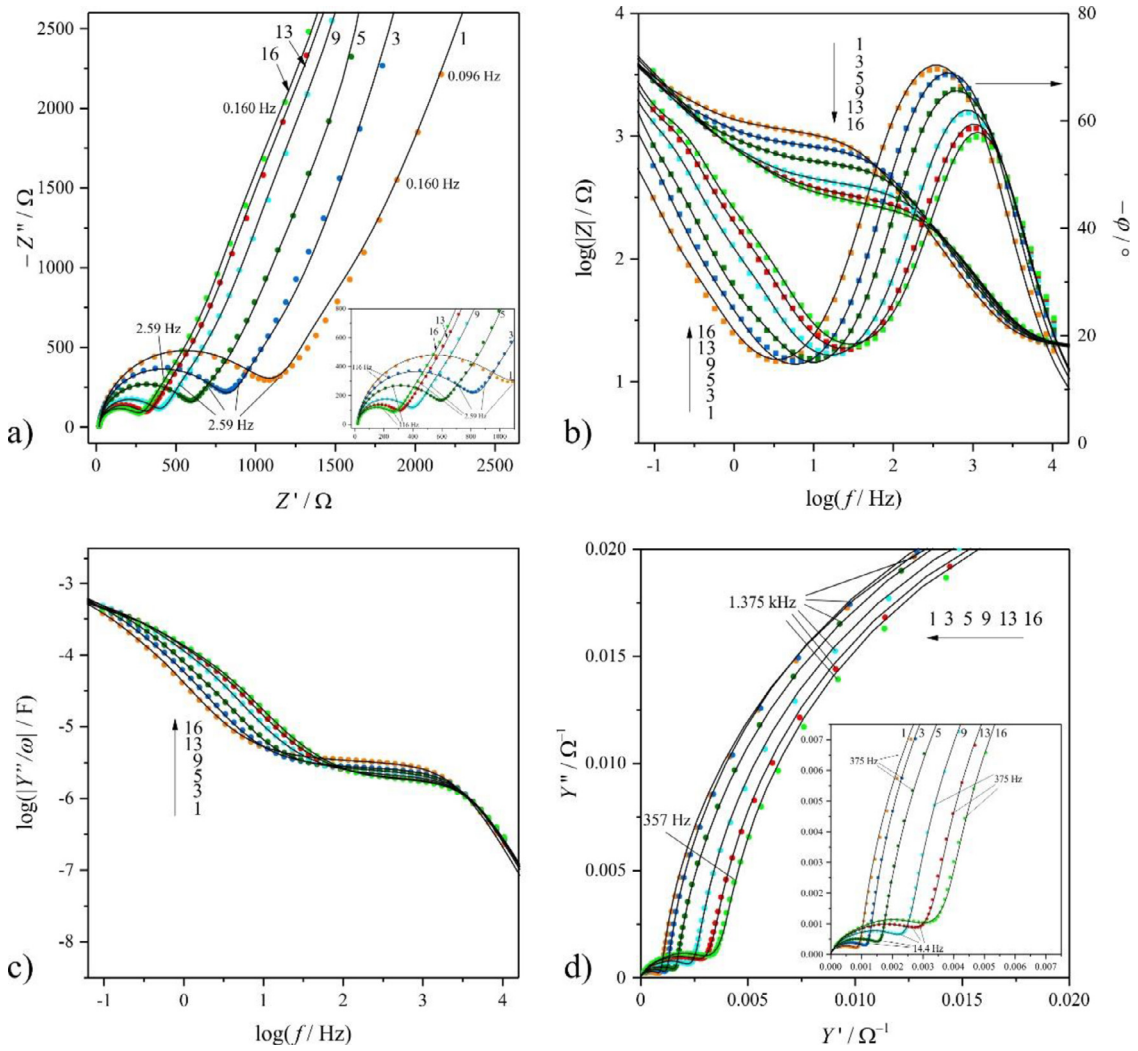

Fig. 14. Selected directly measured ("original") impedance data sets (#1, #3, #5, #9, #13, #16) and the corresponding fitted curves (continuous lines) calculated using the best fit parameters (Table S1 b)). The experimental impedance data points are denoted by dots (•) (or squares (■) in the case of the phase angles in the Bode plot) of different colors. The impedance data sets were recorded for the Au|PEDOT/poly(BPA)|0.1 M H_2SO_4(aq.) electrode (sample E1) successively after overoxidation in the frequency range of f = 50 kHz–96.1 mHz at E = 0.4 V. (a) Complex plane impedance plots (Z ' is the real part and Z " is the imaginary part of the complex impedance), the high frequency regions are shown in the insert, small numbers in the plots refer to frequency values; (b) Bode plots (logarithm of the magnitude (log|Z|) and the phase angle (φ) vs. the logarithm of the frequency (log f)); (c) Logarithm of the absolute value of Y " / ω (the imaginary part of the admittance divided by the angular frequency, sometimes called the "parallel capacitance" of the electrode) as a function of the logarithm of the frequency (log(|Y " / ω| vs. log f), the same data corrected by the estimated ohmic resistance (R_u) are shown in the insert, small numbers in the plots refer to frequency values; (d) Complex admittance plane plots (imaginary part of the admittance (Y ") versus the real part of the admittance (Y ')), the high frequency regions are shown in the insert.

Fig. 16 shows the weighted sum of squares (i.e., the optimized values of the objective function denoted by Q) as a function of time. According to the results the optimum values of the objective functions obtained for the instantaneous impedance spectra and for the sets of measured impedance data differ quite markedly until about 1100 s after the end of the overoxidation process. From the statistical point of view, in this time interval the fit is better in case of the calculated (instantaneous) impedance spectra. After this period, the differences are no longer significant.

Estimated (best fit) parameter values and uncertainties determined for the sequentially recorded impedance data sets (both for the experimentally obtained data and for the instantaneous impedance spectra) are presented in Fig. 17 and Table S1. When comparing the corresponding fitting results for the corrected and uncorrected impedance data it can be seen that the estimates of the parameters R_u, R_{ct}, B, and b differ only slightly in the two cases (see Fig.17a and b). This is also true for the other parameters, if t > 2000 s (Fig. 17c and d). The observed behavior can be well explained by the time evolution of the system, considering, that the values of the parameters R_u, R_{ct}, B, and b are mainly determined by the impedances measured at medium and high frequencies. As the system changes slowly enough, the values recorded at these frequencies are closer to the "true" impedance values corresponding to the stationary state, i.e., to the instantaneous impedance spectra, simply because the time required to determine the impedance data points is sufficiently short. Since the rate of change continuously slows down as time progresses, the differences between the measured and calculated ("instantaneous") impedance values become more and more negligible over time.

The vertical segments (bars) in (a), (b) and (c) indicate the confidence intervals at 95% confidence levels. The confidence intervals for the F parameters are given in Table S1 (a) and (b).

By analyzing the time evolution of the parameters in detail (see Fig. 17a–d), it can be seen that, as expected, the uncompensated ohmic resistance (R_u) remains practically constant during the experiment. The charge transfer resistance (R_{ct}) corresponding to the

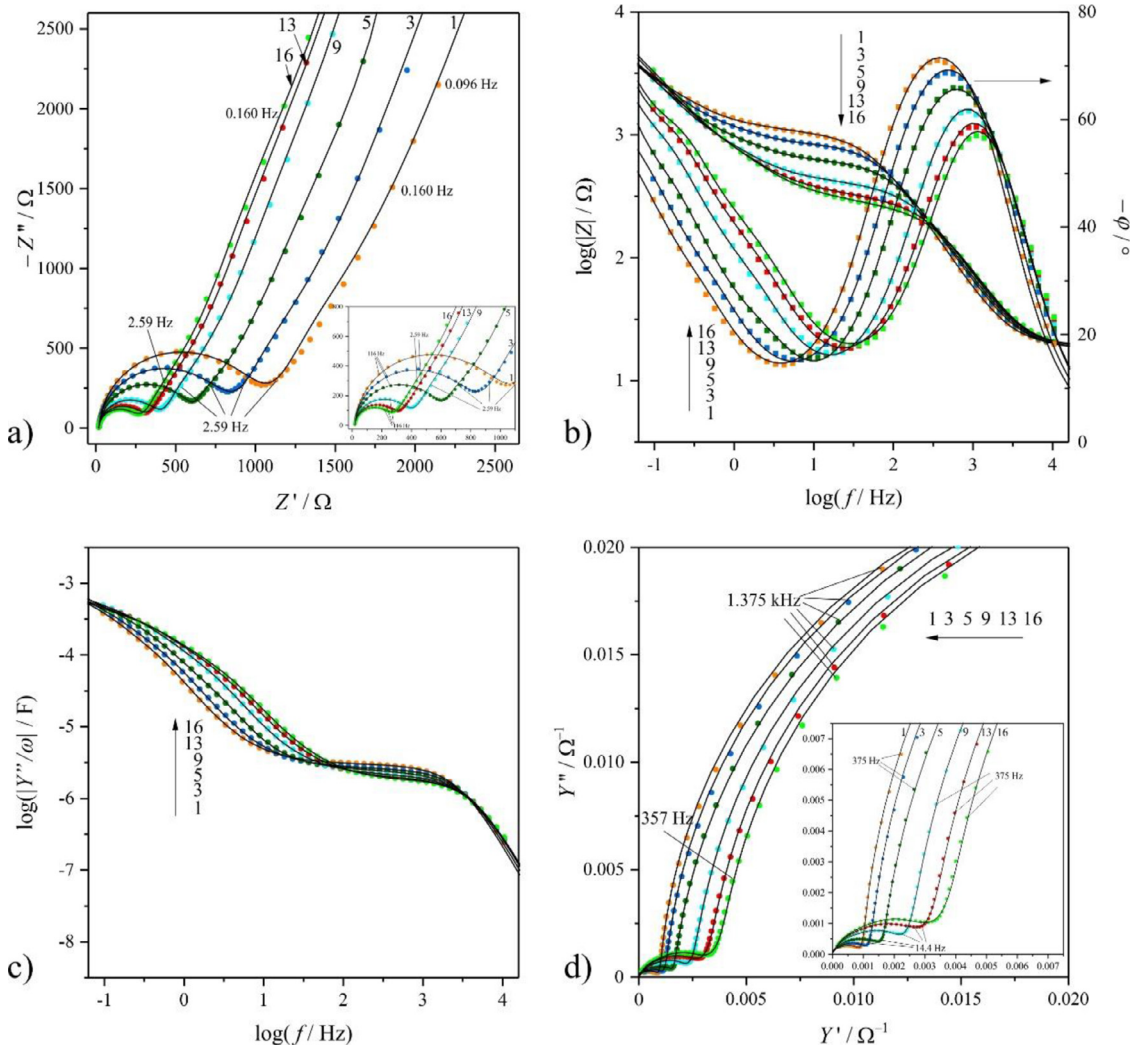

Fig. 15. Instantaneous impedance spectra calculated from the directly measured data sets presented in Fig. 14 (#1, #3, #5, #9, #13, #16) and the corresponding fitted curves (continuous lines) calculated using the best fit parameters (Table S1 c)). The experimental impedance data points are denoted by dots (•) (or squares (■) in the case of the phase angles in the Bode plot) of different colors. (a) Complex plane impedance plots (Z' is the real part and Z'' is the imaginary part of the complex impedance), the high frequency regions are shown in the insert, small numbers in the plots refer to frequency values; (b) Bode plots (logarithm of the magnitude (log|Z|) and the phase angle (φ) vs. the logarithm of the frequency (log f)); (c) Logarithm of the absolute value of Y'' / ω (the imaginary part of the admittance divided by the angular frequency, sometimes called the "parallel capacitance" of the electrode) as a function of the logarithm of the frequency (log($|Y'' / \omega|$ vs. log f), the same data corrected by the estimated ohmic resistance (R_u) are shown in the insert, small numbers in the plots refer to frequency values; (d) Complex admittance plane plots (imaginary part of the admittance (Y'') versus the real part of the admittance (Y')), the high frequency regions are shown in the insert.

time instant just after overoxidation of the film is about 900 Ω. Starting from this value, R_{ct} decreases continuously with experiment time to a terminal value of about 200 Ω. Since the value of the CPE exponent (b) varies between 0.94 and 0.99, the B parameter of the CPE can be regarded as the approximate value of the capacitance of the double layer region at the gold/polymer film interface, which initially decreases with time, and then approaches a limiting value. It should be stressed here that B represents not only the capacitance of the double layer at the substrate/film interface itself but also the capacitance associated with the polymer chains close to the interface [54,59]. As it can be seen from the above results, the direction, dynamics, and nature of the time evolution of R_{ct} and B are consistent with the mechanistic picture suggested in Refs. [20,22], according to which during overoxidation a significant fraction of the polymer chains become detached from the substrate surface, while at electrode potentials more negative than those at which overoxidation takes place the readsorption of the polymer chains (polymer chain ends) becomes possible. This can also be formulated as follows: the "effective" coverage of the substrate by the polymer decreases during overoxidation, and the coverage starts to increase again when the potential is held in an appropriate potential range. Obviously, the first process leads to an increase, and the second to a decrease of the charge transfer resistance. The other parameters, namely P_1, F_1, F_2, F_3, and F_4, depend mainly on the characteristics of the "bulk" of the polymer layer, especially on its morphology and transport properties. The time evolution of the best fit parameter estimates is shown in Fig.17c and d, however, contrary to what we expected on the basis of the above simple delamination/readsorption model [20–22], these parameters do not change monotonically over time, and sudden changes in the parameter values is observed at $t = 1371$ s. This suggests that something happened around this time inside the polymer layer, most likely structural changes of the polymer chains or formation of cracks due to the evolution of internal stress. In contrast, it is highly unlikely that the (sudden) decrease of the parameter values is caused by an increase in the value of the effective diffusion coefficient (D^*). (Formally, the observed changes in the values of the P_1 and F_i parameters could also be explained by the increase of D^*

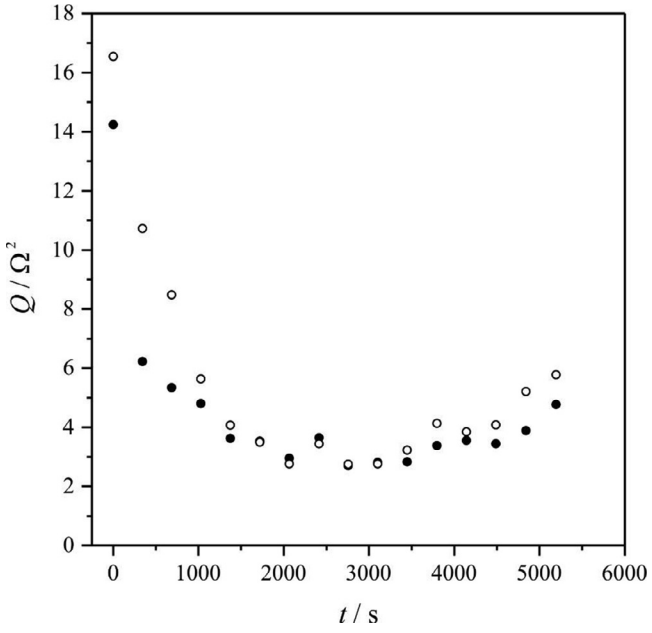

Fig. 16. The optimized values of the objective functions (weighted sum of squares, Q) resulting from the parameter estimation procedures as a function of time (see Table S1). The Q values belonging to the directly measured ("original") impedance data sets recorded for the Au|PEDOT/poly(BPA)|0.1 M H_2SO_4(aq.) electrode are denoted by (○), the Q values belonging to the instantaneous impedance spectra obtained using the 4-dimensional analysis method are denoted by (●).

since they are inversely proportional to the square route of D^*.) Instead, the observed behavior may somehow be related to changes in the conjugation length of the PEDOT backbone, however, further investigations are needed to understand the background of this issue.

5. Concluding remarks

One of the most important results of the present work is that the electrochemical deposition of poly(BPA) on the PEDOT layer in a PEDOT modified gold electrode results in an improved stability of the system against the adverse effects of overoxidation. It is well known that overoxidation of polymer films in polymer modified electrodes is very often accompanied by delamination at the film/substrate interface making the unit unusable. For instance, the observed results indicate a significant improvement of the mechanical stability of the polymer structures, resulting in a more adherent layer and reduced degradation. Another important feature is that both polymers can be deposited electrochemically. The above findings suggest that poly(BPA)-like polymers can be effectively used to enhance the electrochemical/mechanical properties of conductive polymer fibers, microwires and bundles as well, and therefore the combination of poly(BPA) and PEDOT (or more generally the combination of electrochemically deposited conducting and non-conducting polymers) offer some potential e.g. for biomedical applications (see e.g. [89,90]).

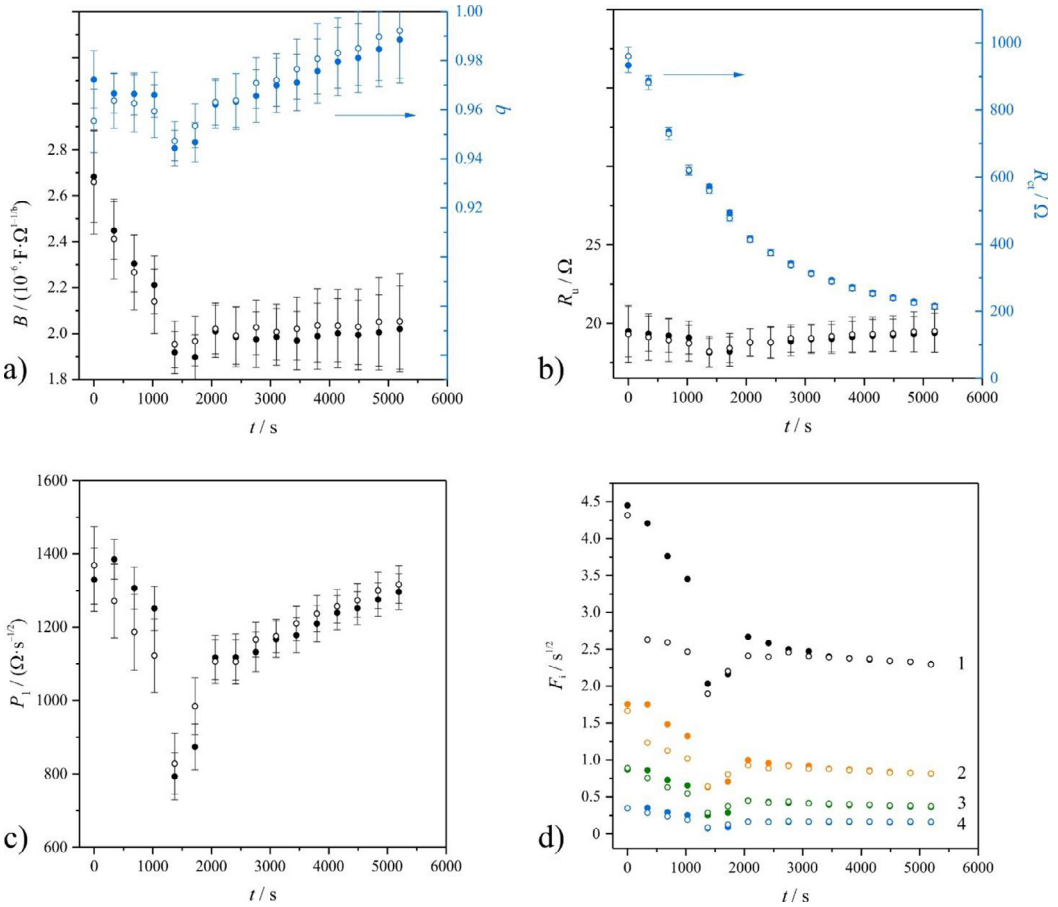

Fig. 17. The estimated (best fit) parameter values as a function of time (t). (a) the B parameter values of the CPE in Eq. (23) and the corresponding CPE exponents. Since the CPE exponents (b) are close to unity, B can be regarded as the approximate value of the capacitance of the double layer region at the gold/polymer film interface; (b) The ohmic resistance (R_u) and charge transfer resistance (R_{ct}); (c) The parameter of the finite-length transport impedance P_1; (d) The F parameters (F_1, F_2, F_3, and F_4). The parameter values resulting from the fitting of the directly measured ("original") impedance data sets recorded for the Au|PEDOT/poly(BPA)|0.1 M H_2SO_4(aq.) electrode are denoted by (○), the values obtained from the fitting of the instantaneous impedance spectra are denoted by (●).

Another interesting finding is that in case of PEDOT and poly(BPA)/PEDOT modified gold electrodes the deviations of the impedance responses from the purely capacitive behavior predicted at low frequencies by the theoretical models can be well explained solely by the assumption of uneven film thickness. The impedance model, which takes into account the film thickness distribution (by assuming 4 regions of different film thicknesses on the basis of SEM micrographs) gives a good description of the impedance data recorded for Au | PEDOT | 0.1 mol/dm^3 H_2SO_4(aq.) and Au | [poly(BPA)/PEDOT] | 0.1 mol/dm^3 H_2SO_4(aq.) electrodes. By using this model reasonable values for the different parameters characterizing the polymer film electrodes could be obtained by fitting the impedance function to the experimental EIS data. To our knowledge this is the first report on a successful wide frequency range parameter estimation based on an expression (impedance model) which includes explicitly the effect of thickness distribution on the impedance response of polymer modified electrodes.

Similarly to overoxidized PEDOT modified electrodes, time evolution of the electrochemical properties of the poly(BPA)/PEDOT films could be observed after overoxidation. This means that the system is intrinsically nonstationary and is affected by time-dependent phenomena. As a consequence, the sequentially recorded sets of "impedance" data (that is the experimental data measured over a frequency range using the consecutive frequency sweep mode) change slowly, but continuously over several hours when the electrode potential is held in the "stability region" after overoxidation of the film. The four-dimensional analysis method and complex nonlinear least-squares (CNLS) fitting has been successfully used for the estimation of the impedance parameters corresponding to time instants after overoxidation of the polymer film. The results confirmed (again) that the 4D analysis technique is very well suited for "slow" non-stationarities [39].

Declaration of Competing Interest

The authors declare that they have no known competing financial interests or personal relationships that could have appeared to influence the work reported in this paper.

Credit authorship contribution statement

Krisztina J. Szekeres: Conceptualization, Methodology, Investigation, Formal analysis, Visualization, Validation, Writing – original draft, Funding acquisition. **Mária Ujvári:** Methodology, Resources. **Soma Vesztergom:** Software, Data curation, Funding acquisition. **Gyözö G. Láng:** Conceptualization, Methodology, Investigation, Formal analysis, Software, Visualization, Writing – review & editing, Funding acquisition, Supervision.

Acknowledgments

Financial support from the National Research, Development, and Innovation Office (NKFIH, Grant Nos. K129210 and FK135375) is gratefully acknowledged. The work within project no. VEKOP-2.3.2-16-2017-00013 and the ELTE Institutional Excellence Program (TKP2020-IKA-05) was financed by the European Union and the Hungarian Ministry of Human Capacities. The work was also supported by the ÚNKP-20-3 New National Excellence Program of the Ministry for Innovation and Technology from the source of the National Research, Development, and Innovation Fund.

Supplementary materials

Supplementary material associated with this article can be found, in the online version, at doi:10.1016/j.electacta.2021.138975.

Appendix A

In terms of the exponential function e^x the hyperbolic tangent and cotangent functions can be expressed as

$$\coth x = \frac{e^x + e^{-x}}{e^x - e^{-x}}, \quad x \neq 0 \tag{A1}$$

and

$$\tanh x = \frac{e^x - e^{-x}}{e^x + e^{-x}}. \tag{A2}$$

On the other hand,

$$\coth\left(\frac{x}{2}\right) = \frac{e^{x/2} + e^{-x/2}}{e^{x/2} - e^{-x/2}}, \quad x \neq 0 \tag{A3}$$

and

$$\tanh\left(\frac{x}{2}\right) = \frac{e^{x/2} - e^{-x/2}}{e^{x/2} + e^{-x/2}}. \tag{A4}$$

Consequently, the sum of the above two functions can be written as

$$\coth\left(\frac{x}{2}\right) + \tanh\left(\frac{x}{2}\right) = \frac{e^{x/2} + e^{-x/2}}{e^{x/2} - e^{-x/2}} + \frac{e^{x/2} - e^{-x/2}}{e^{x/2} + e^{-x/2}} = 2\frac{e^x + e^{-x}}{e^x - e^{-x}} = 2\coth x. \tag{A5}$$

Appendix B

The Taylor series of the coth x fuction is (B_{2n} denotes Bernoulli numbers)

$$\coth x = \frac{1}{x} + \frac{x}{3} - \frac{x^3}{45} + \frac{x^5}{945} + \cdots = \sum_0^\infty \frac{(-1)^{n+1} 2^{2n} B_{2n} x^{2n-1}}{(2n)!}, \quad 0 < |x| < \pi \tag{B1}$$

This means that at low frequencies the $\frac{P_i}{s}\coth[\frac{L_i s}{\sqrt{D^*}}]$ ($= \frac{P_i}{s}\coth[F_i s]$) terms (that determine the impedance in this regime) in Eq. (16) can be well approximated by

$$\frac{P_i}{s}\frac{1}{F_i s} = \frac{P_i}{(\mathrm{i}\omega)^{1/2}}\frac{1}{F_i(\mathrm{i}\omega)^{1/2}} = \frac{P_i}{F_i}(\mathrm{i}\omega)^{-1} = \left(\mathrm{i}\omega C_{i,\mathrm{L}}\right)^{-1}. \tag{B2}$$

The so called "low frequency capacitance" of the system is then:

$$C_\mathrm{L} = \sum_i C_{i,\mathrm{L}} \tag{B3}$$

References

[1] J. Isaksson, Organic Bioelectronics - Electrochemical Devices based on Conjugated Polymers, LiU-Tryck, 2007.
[2] X. Li, Y. Wang, X. Yang, J. Chen, H. Fu, T. Cheng, Y. Wang, Conducting polymers in environmental analysis, TrAC Trends Anal. Chem. 39 (2012) 163–179, doi:10.1016/j.trac.2012.06.003.
[3] G. Inzelt, Conducting Polymers (A New Era in Electrochemistry), 2nd ed., Springer, Berlin, Heidelberg, 2012.
[4] G. Inzelt, Recent advances in the field of conducting polymers, J. Solid State Electrochem. 21 (2017) 1965–1975, doi:10.1007/s10008-017-3611-6.
[5] K.J. Szekeres, K. Hegedüs, M. Ujvári, G.G. Láng, Investigation of the electrochemical properties of poly(3,4-ethylenedioxypyrrole) films electrodeposited from aqueous solutions, J. Electroanal. Chem. 826 (2018) 16–22, doi:10.1016/j.jelechem.2018.08.017.
[6] A.D. Aguilar, E.S. Forzani, M. Leright, F. Tsow, A. Cagan, R.A. Iglesias, L.A. Nagahara, I. Amlani, R. Tsui, N.J. Tao, A hybrid nanosensor for TNT vapor detection, Nano Lett. 10 (2010) 380–384, doi:10.1021/nl902382s.
[7] J. Jang, M. Chang, H. Yoon, Chemical sensors based on highly conductive poly(3,4-ethylene- dioxythiophene) nanorods, Adv. Mater. 17 (2005) 1616–1620, doi:10.1002/adma.200401909.
[8] K. Dunst, J. Karczewski, P. Jasiński, Nitrogen dioxide sensing properties of PEDOT polymer films, Sens. Actuators B 247 (2017) 108–113, doi:10.1016/j.snb.2017.03.003.

[9] J. Yang, D.H. Kim, J.L. Hendricks, M. Leach, R. Northey, D.C. Martin, Ordered surfactant-templated poly(3,4-ethylenedioxythiophene) (PEDOT) conducting polymer on microfabricated neural probes, Acta Biomater. 1 (2005) 125–136, doi:10.1016/j.actbio.2004.09.006.

[10] A. Özcan, S. Ilkbaş, Preparation of poly(3,4-ethylenedioxythiophene) nanofibers modified pencil graphite electrode and investigation of over-oxidation conditions for the selective and sensitive determination of uric acid in body fluids, Anal. Chim. Acta 891 (2015) 312–320, doi:10.1016/j.aca.2015.08.015.

[11] J.M. Lin, Y.L. Su, W.T. Chang, W.Y. Su, S.H. Cheng, Strong adsorption characteristics of a novel overoxidized poly(3,4-ethylenedioxythiophene) film and application for dopamine sensing, Electrochim. Acta 149 (2014) 65–75, doi:10.1016/j.electacta.2014.10.030.

[12] N. Rozlosnik, New directions in medical biosensors employing poly(3,4-ethylenedioxy thiophene) derivative-based electrodes, Anal. Bioanal. Chem. 395 (2009) 637–645, doi:10.1007/s00216-009-2981-8.

[13] D.C. Martin, Molecular design, synthesis, and characterization of conjugated polymers for interfacing electronic biomedical devices with living tissue, MRS Commun. 5 (2015) 131–153, doi:10.1557/mrc.2015.17.

[14] S. Nagane, P. Sitarik, Y. Wu, Q. Baugh, S. Chhatre, J. Lee, D.C. Martin, Functionalized polythiophene copolymers for electronic biomedical devices, MRS Adv. 5 (2020) 943–956, doi:10.1557/adv.2020.3.

[15] A. Zykwinska, W. Domagala, B. Pilawa, M. Lapkowski, Electrochemical overoxidation of poly(3,4-ethylenedioxythiophene) - PEDOT studied by means of in situ ESR spectroelectrochemistry, Electrochim. Acta 50 (2005) 1625–1633, doi:10.1016/j.electacta.2004.10.026.

[16] M. Ujvári, M. Takács, S. Vesztergom, F. Bazsó, F. Ujhelyi, G.G. Láng, Monitoring of the electrochemical degradation of PEDOT films on gold using the bending beam method, J. Solid State Electrochem. 15 (2011) 2341–2349, doi:10.1007/s10008-011-1472-y.

[17] G.G. Láng, M. Ujvári, F. Bazsó, S. Vesztergom, F. Ujhelyi, In situ monitoring of the electrochemical degradation of polymer films on metals using the bending beam method and impedance spectroscopy, Electrochim. Acta 73 (2012) 59–69.

[18] M. Ujvári, J. Gubicza, V. Kondratiev, K.J. Szekeres, G.G. Láng, Morphological changes in electrochemically deposited poly(3,4-ethylenedioxythiophene) films during overoxidation, J. Solid State Electrochem. 19 (2015) 1247–1252, doi:10.1007/s10008-015-2746-6.

[19] G.G. Láng, M. Ujvári, S. Vesztergom, V. Kondratiev, J. Gubicza, K.J. Szekeres, The electrochemical degradation of poly(3,4-ethylenedioxythiophene) films electrodeposited from aqueous solutions, Z. Phys. Chem. 281 (2016) 1281–1302, doi:10.1515/zpch-2016-0752.

[20] D. Zalka, N. Kovács, K. Szekeres, M. Ujvári, S. Vesztergom, S. Eliseeva, V. Kondratiev, G.G. Láng, Determination of the charge transfer resistance of poly(3,4-ethylenedioxythiophene)-modified electrodes immediately after overoxidation, Electrochim. Acta 247 (2017) 321–332, doi:10.1016/j.electacta.2017.06.177.

[21] M. Ujvári, D. Zalka, S. Vesztergom, S. Eliseeva, V. Kondratiev, G.G. Láng, Electrochemical impedance measurements in non-stationary systems - application of the 4-dimensional analysis method for the impedance analysis of overoxidized poly(3,4-ethylenedioxythiophene)-modified electrodes, Bulg. Chem. Commun. 49 (2017) 106–113.

[22] D. Zalka, S. Vesztergom, M. Ujvári, G.G. Láng, Electrochemical behaviour of poly(3,4-ethylenedioxytiophene) modified glassy carbon electrodes after overoxidation — the influence of the substrate on the charge transfer resistance, J. Electrochem. Sci. Eng. 8 (2018) 151–162, doi:10.5599/jese.508.

[23] Q. Pei, O. Inganäs, Electrochemical applications of the bending beam method. 1. Mass transport and volume changes in polypyrrole during redox, J. Phys. Chem. 96 (1992) 10507–10514, doi:10.1021/j100204a071.

[24] Q. Pei, O. Inganäs, Electrochemical applications of the bending beam method. 2. Electroshrinking and slow relaxation in polypyrrole, J. Phys. Chem. 97 (1993) 6034–6041, doi:10.1021/j100124a041.

[25] M. Seo, Electro-Chemo-Mechanical Properties of Solid Electrode Surfaces, Springer, Singapore, 2020, doi:10.1007/978-981-15-7277-7.

[26] Y. Hui, C. Bian, J. Wang, J. Tong, S. Xia, Comparison of two types of overoxidized PEDOT films and their application in sensor fabrication, Sensors 17 (2017) 628, doi:10.3390/s17030628.

[27] K.J. Szekeres, É. Fekete, M. Ujvári, S. Vesztergom, V.V. Kondratiev, G.G. Láng, Some observations on the electrochemical reactions of bisphenol A on polycrystalline gold in contact with 0.1 M aqueous $NaClO_4$ solution, Russ. J. Electrochem. 55 (2019) 1127–1135, doi:10.1134/S1023193519110132.

[28] X. Li, Y. Cui, Y. Feng, Z. Xie, J. Gu, Reaction pathways and mechanisms of the electrochemical degradation of phenol on different electrodes, Water Res. 39 (2005) 1972–1981, doi:10.1016/j.watres.2005.02.021.

[29] G. Mengoli, M.M. Musiani, Protective coatings on iron by anodic oxidation of phenols in oxalic acid medium, Electrochim. Acta 31 (1986) 201–210, doi:10.1016/0013-4686(86)87109-2.

[30] H. Kuramitz, Y. Nakata, M. Kawasaki, S. Tanaka, Electrochemical oxidation of bisphenol A. Application to the removal of bisphenol A using a carbon fiber electrode, Chemosphere 45 (2001) 37–43, doi:10.1016/S0045-6535(01)00032-7.

[31] Y. Cui, X. Li, G. Chen, Electrochemical degradation of bisphenol A on different anodes, Water Res. 43 (2009) 1968–1976, doi:10.1016/j.watres.2009.01.026.

[32] E. Mazzotta, C. Malitesta, E. Margapoti, Direct electrochemical detection of bisphenol A at PEDOT-modified glassy carbon electrodes, Anal. Bioanal. Chem. 405 (2013) 3587–3592, doi:10.1007/s00216-013-6723-6.

[33] K. Varmira, M. Saed-Mocheshi, A.R. Jalalvand, Electrochemical sensing and bio-sensing of bisphenol A and detection of its damage to DNA: a comprehensive review, Sens. Bio Sen. Res. 15 (2017) 17–33, doi:10.1016/j.sbsr.2017.07.002.

[34] G.G. Láng, M. Ujvári, Z. Dankházi, S. Vesztergom, K.J. Szekeres, Analysis of impedance spectra of electrochemically deposited PEDOT films recorded before and after overoxidation, Proceeding of the 10th International Symposium on Electrochemical Impedance Spectroscopy, 2016 A Toxa.

[35] G.G. Láng, D. Zalka, On the correct use of stepped-sine excitations for the measurement of time-varying bioimpedance, Physiol. Meas. 39 (2018) aaab0f, doi:10.1088/1361-6579/aaab0f.

[36] G.G. Láng, K.J. Szekeres, M. Ujvári, S. Vesztergom, Electrochemical impedance spectroscopy for the characterization of conductive polymer films – The non-stationary case, Proceeding of the 71st Annual Meeting of the International Society of Electrochemistry, 2020 http://ise-2020-symposium17.fkit.hr/?page_id=132.

[37] C.A. Schiller, F. Richter, E. Gülzow, N. Wagner, Validation and evaluation of electrochemical impedance spectra of systems with states that change with time, Phys, Chem. Chem. Phys. 3 (2001) 374–378, doi:10.1039/b007678n.

[38] N. Wagner, E. Gülzow, Change of electrochemical impedance spectra (EIS) with time during CO-poisoning of the Pt-anode in a membrane fuel cell, J. Power Sources 127 (2004) 341–347, doi:10.1016/j.jpowsour.2003.09.031.

[39] K.J. Szekeres, S. Vesztergom, M. Ujvári, G.G. Láng, Some methods for the determination of valid impedance spectra in non-stationary electrochemical systems – concepts and techniques of practical importance, ChemElectroChem 8 (2021) 1233–1250, doi:10.1002/celc.202100093.

[40] Z.B. Stoynov, B.S. Savova-Stoynov, Impedance study of non-stationary systems: four-dimensional analysis, J. Electroanal. Chem. 183 (1985) 133–144, doi:10.1016/0368-1874(85)85486-1.

[41] B. Savova-Stoynov, Z.B. Stoynov, Four-dimensional estimation of the instantaneous impedance, Electrochim. Acta 37 (1992) 2353–2355, doi:10.1016/0013-4686(92)85131-4.

[42] Z. Stoynov, Nonstationary impedance spectroscopy, Electrochim. Acta 38 (1993) 1919–1922, doi:10.1016/0013-4686(93)80315-Q.

[43] C. Gabrielli, H. Takenouti, O. Haas, A. Tsukada, Impedance investigation of the charge transport in film-modified electrodes, J. Electroanal. Chem. 302 (1991) 59–89, doi:10.1016/0022-0728(91)85032-K.

[44] G. Láng, G. Inzelt, Some problems connected with impedance analysis of polymer film electrodes : effect of the film thickness and the thickness distribution, Electrochim. Acta 36 (1991) 847–854, doi:10.1016/0013-4686(91)85284-E.

[45] M.F. Mathias, O. Haas, Effect of counterion type on charge transport at redox polymer-modified electrodes, J. Phys. Chem. 97 (1993) 9217–9225, doi:10.1021/j100138a025.

[46] K.L. Brown, R. Danforth, E. Bleitz, Y.H.D. Rens, Cyclic voltammetric and spectroelectrochemical studies of Tris(5-amino-1,10-phenantroline)Iron(II) Polymer Films, Int. J. Electrochem. Sci. 15 (2020) 10707–10721, doi:10.20964/2020.11.66.

[47] I. Ivanko, J. Pánek, J. Svoboda, A. Zhigunov, E. Tomšík, Tuning the photoluminescence and anisotropic structure of PEDOT, J. Mater. Chem. C 7 (2019) 7013–7019, doi:10.1039/c9tc00955h.

[48] W.J. Albery, C.M. Elliott, A.R. Mount, A transmission line model for modified electrodes and thin layer cells, J. Electroanal. Chem. 288 (1990) 15–34.

[49] R.D. Armstrong, Impedance plane display for an electrode with diffusion restricted to a thin layer, J. Electroanal. Chem. 198 (1986) 177–180.

[50] G. Inzelt, G. Láng, Impedance analysis of poly(tetracyanoquinodimethane) electrodes: effect of electrolyte concentration and temperature, Electrochim. Acta 36 (1991) 1355–1361.

[51] C. Deslouis, M.M. Musiani, B. Tribollet, Ac impedance study of transport processes in polyaniline membranes, J. Phys. Chem. 98 (1994) 2936–2940, doi:10.1021/j100062a033.

[52] S. Fletcher, An electrical model circuit that reproduces the behaviour of conducting polymer electrodes in electrolyte solutions, J. Electroanal. Chem. 337 (1992) 127–145, doi:10.1016/0022-0728(92)80533-A.

[53] G. Inzelt, G. Láng, Model dependence and reliability of the electrochemical quantities derived from the measured impedance spectra of polymer modified electrodes, J. Electroanal. Chem. 378 (1994) 39–49, doi:10.1016/0022-0728(94)87055-1.

[54] G.G. Láng, M. Ujvári, G. Inzelt, Possible origin of the deviation from the expected impedance response of polymer film electrodes, Electrochim. Acta 46 (2001) 4159–4175, doi:10.1016/S0013-4686(01)00704-6.

[55] M.F. Mathias, O. Haas, An alternating current impedance model including migration and redox-site interactions at polymer-modified electrodes, J. Phys. Chem. 96 (1992) 3174–3182, doi:10.1021/j100186a073.

[56] M.A. Vorotyntsev, C. Deslouis, M.M. Musiani, B. Tribollet, K. Aoki, Transport across an electroactive polymer film in contact with media allowing both ionic and electronic interfacial exchange, Electrochim. Acta 44 (1999) 2105–2115, doi:10.1016/S0013-4686(98)00318-1.

[57] M.A. Vorotyntsev, J.-P. Badiali, G. Inzelt, Electrochemical impedance spectroscopy of thin films with two mobile charge carriers: effects of the interfacial charging, J. Electroanal. Chem. 472 (1999) 7–19, doi:10.1016/S0022-0728(99)00253-3.

[58] J. Bisquert, G. Garcia-Belmonte, F. Fabregat-Santiago, N.S. Ferriols, P. Bogdanoff, E.C. Pereira, Doubling exponent models for the analysis of porous film electrodes by impedance. Relaxation of TiO_2 nanoporous in aqueous solution, J. Phys. Chem. B 104 (2000) 2287–2298, doi:10.1021/jp993148h.

[59] G.G. Láng, M. Ujvári, T.A. Rokob, G. Inzelt, The brush model of the polymer films — analysis of the impedance spectra of Au,Pt|poly (o-phenylenediamine) electrodes, Electrochim. Acta 51 (2006) 1680–1694, doi:10.1016/j.electacta.2005.02.100.

[60] G. Inzelt, G.G. Láng, Electrochemical impedance spectroscopy (EIS) for polymer characterization, in: S. Cosnier, A. Karyakin (Eds.), Electropolymerization (Concepts, Materials and Applications), WILEY-VCH Verlag GmbH & Co. KGaA, Weinheim, Germany, 2010.
[61] J. Bisquert, G. Garcia-Belmonte, P. Bueno, E. Longo, L.O.S. Bulhões, Impedance of constant phase element (CPE)-blocked diffusion in film electrodes, J. Electroanal. Chem. 452 (1998) 229–234, doi:10.1016/S0022-0728(98)00115-6.
[62] J. Bisquert, G. Garcia-Belmonte, F. Fabregat-Santiago, P.R. Bueno, Theoretical models for ac impedance of finite diffusion layers exhibiting low frequency dispersion, J. Electroanal. Chem. 475 (1999) 152–163, doi:10.1016/S0022-0728(99)00346-0.
[63] G. Garcia-Belmonte, J. Bisquert, Impedance analysis of galvanostatically synthesized polypyrrole films. Correlation of ionic diffusion and capacitance parameters with the electrode morphology, Electrochim. Acta 47 (2002) 4263–4272, doi:10.1016/S0013-4686(02)00510-8.
[64] G.G. Láng, L. Kocsis, G. Inzelt, Application of the Kramers-Kronig transformation for the data validation of impedance spectra of electroactive polymer films on electrodes, Electrochim. Acta 38 (1993) 1047–1049, doi:10.1016/0013-4686(93)87026-A.
[65] L.F.Q.P. Marchesi, F.R. Simoes, L.A. Pocrifka, E.C. Pereira, Investigation of polypyrrole degradation using electrochemical impedance spectroscopy, J. Phys. Chem. 115 (2011) 9570–9575, doi:10.1021/jp2041263.
[66] G.G. Láng, G. Inzelt, An advanced model of the impedance of polymer film electrodes, Electrochim. Acta 44 (1999) 2037–2051, doi:10.1016/S0013-4686(98)00312-0.
[67] I. Rubinstein, J. Rishpon, S. Gottesfeld, An AC-impedance study of electrochemical processes at nafion-coated electrodes, J. Electrochem. Soc. 133 (1986) 729–734, doi:10.1149/1.2108663.
[68] L. "Bert" Groenendaal, F. Jonas, D. Freitag, H. Pielartzik, J.R. Reynolds, Poly(3,4-ethylenedioxythiophene) and its derivatives: past, present, and future, Adv. Mater. 12 (2000) 481–494 10.1002/(SICI)1521-4095(200004)12:7<481::AID-ADMA481>3.0.CO;2-C.
[69] B. Winther-Jensen, K. West, Vapor-Phase polymerization of 3,4-ethylenedioxythiophene: a route to highly conducting polymer surface layers, Macromolecules 37 (2004) 4538–4543, doi:10.1021/ma049864l.
[70] O. Contamin, E. Levart, G. Magner, R. Parsons, M. Savy, Restricted diffusion impedance. Theory and application to the reaction of oxygen on a hydrogen phthalocyanine film, J. Electroanal. Chem. 179 (1984) 41–52, doi:10.1016/S0022-0728(84)80273-9.
[71] C. Gabrielli, O. Haas, H. Takenouti, Impedance analysis of electrodes modified with a reversible redox polymer film, J. Appl. Electrochem. 17 (1987) 82–90, doi:10.1007/BF01009134.
[72] J.R. Macdonald, D.R. Franceschetti, Precision of impedance spectroscopy estimates of bulk, reaction rate, and diffusion parameters, J. Electroanal. Chem. 307 (1991) 1–11, doi:10.1016/0022-0728(91)85534-V.
[73] J. Bobacka, A. Lewenstam, A. Ivaska, A. Fin, Electrochemical impedance spectroscopy of oxidized poly(3,4-ethylenedioxythiophene) film electrodes in aqueous solutions, J. Electroanal. Chem. 489 (2000) 17–27, doi:10.1016/S0022-0728(00)00206-0.
[74] M.R. Abidian, D.C. Martin, Experimental and theoretical characterization of implantable neural microelectrodes modified with conducting polymer nanotubes, Biomaterials 29 (2008) 1273–1283, doi:10.1016/j.biomaterials.2007.11.022.
[75] C. de Boor, A Practical Guide to Splines, Springer, New York, 2001 Applied Ma.
[76] P. Valkó, S. Vajda, Advanced Scientific Computing in BASIC with Applications in Chemistry, Biology and Pharmacology, Elsevier, Amsterdam, 1989 Data handl.
[77] Installer package of the software for the correction of "impedance" data measured under non-stationary conditions, (2020). http://electro.chem.elte.hu:5080/members/vesztergom/index_en.htm.
[78] K. Levenberg, A Method for the solution of certain non-linear problems in least squares, Q. Appl. Math. 2 (1944) 164–168.
[79] D.W. Marquardt, An algorithm for least-squares estimation of nonlinear parameters, SIAM J. Appl. Math. 11 (1963) 431–441.
[80] T. Komura, T. Yamaguti, K. Takahasi, Impedance Study of the charge transport at poly-o-phenylenediamine film electrodes, Electrochim. Acta 41 (1996) 2865–2870, doi:10.1016/0013-4686(96)00114-4.
[81] B.W. Silverman, Density Estimation for Statistics and Data Analysis, First CRC, Chapman & Hall/CRC, London, UK, 1998.
[82] G.G. Láng, Interface stress measurements in an electrochemical environment, in: K. Wandelt (Ed.), Encyclopedia of Interfacial Chemistry Surface Science and Electrochemistry, 1st ed., Elsevier, New York (NY), Amsterdam, London, Tokyo, 2018, pp. 195–206.
[83] G.G. Láng, C. Barbero, Laser techniques for the study of electrode processes, in: F. Scholz (Ed.), Monographs in Electrochemistry, Springer-Verlag, Berlin Heidelberg, 2012, doi:10.1007/978-3-642-27651-4.
[84] G.G. Láng, Comment on "*in situ* measurements of stress-potential coupling in lithiated silicon" [J. Electrochem. Soc., 157, A1253 (2010)], "On plastic deformation and fracture in si films during electrochemical lithiation/delithiation cycling" [J. Electrochem. Soc., 162, A2840 (2015)], J. Electrochem. Soc. 163 (2016) Y15, doi:10.1149/2.0321607jes.
[85] M. Ujvári, G.G. Láng, S. Vesztergom, K.J. Szekeres, N. Kovács, J. Gubicza, Structural changes during the overoxidation of electrochemically deposited poly(3,4-ethylenedioxythiophene) films, J. Electrochem. Sci. Eng. 6 (2016) 77–89, doi:10.5599/jese.225.
[86] M. Ujvári, S. Vesztergom, C.B. Pénzes, G.G. Láng, Changes of the interfacial stress with electrode potential in the Ru|0.1 M perchloric acid system, Electrochem. Commun. 28 (2013) 111–113, doi:10.1016/j.elecom.2012.12.023.
[87] G.G. Láng, N. Kovács, S. Vesztergom, M. Ujvári, D. Zalka, K. Szekeres, Experimental methods for the determination of stress changes at electrified solid-liquid interfaces, Tech. Mess. 84 (2017) 644–658, doi:10.1515/teme-2016-0082.
[88] B. Cain, P.L. Schechter, M.W. Bautz, Measuring gravitational lensing flexion in A1689 using an analytic image model, Astrophys. J. 736 (2011) 43, doi:10.1088/0004-637X/736/1/43.
[89] M.J. Donahue, A. Sanchez-Sanchez, S. Inal, J. Qu, R.M. Owens, D. Mecerreyes, G.G. Malliaras, D.C. Martin, Tailoring PEDOT properties for applications in bioelectronics, Mater. Sci. Eng. R 140 (2020) 100546, doi:10.1016/j.mser.2020.100546.
[90] AmericanChemicalSociety, Cyborg" technology could enable new diagnostics, merger of humans and AI, Sci. Daily (2020), https://www.sciencedaily.com/releases/2020/08/200817104315.htm.